STRESS TENSOR IN REAL-SPACE KOHN-SHAM DENSITY FUNCTIONAL THEORY

A Dissertation
Presented to
The Academic Faculty

By

Abhiraj Sharma

In Partial Fulfillment
of the Requirements for the Degree
Master of Science in the
College of Engineering
Department of Civil and Environmental Engineering

Georgia Institute of Technology

May 2021

STRESS TENSOR IN REAL-SPACE KOHN-SHAM DENSITY FUNCTIONAL THEORY

Thesis committee:

Dr. Phanish Suryanarayana
Department of Civil and Environmental Engineering
Georgia Institute of Technology

Dr. Ting Zhu
The George W. Woodruff School of Mechanical Engineering
Georgia Institute of Technology

Dr. Arash Yavari
Department of Civil and Environmental Engineering
Georgia Institute of Technology

Date approved: 16 March, 2021

Knowledge exists, man only discovers it.

Swami Vivekananda

Dedicated to my parents

ACKNOWLEDGMENTS

Firstly, I would like to thank my advisor Dr. Phanish Suryanarayana for trusting me with this challenging research problem and helping in my research endeavor by providing valuable suggestions and engaging in interactive brainstorming sessions. I would also like to thank Dr. Arash Yavari and Dr. Ting Zhu for serving on my thesis committee and providing valuable feebacks on my thesis.

Special thanks are due to the friends and colleagues who made this work possible. I would like to thank my group members Qimen Xu and Dr. Mostafa F. Shojaei who were invaluable both as friends and as research colleagues. I would also like to thank my flatmates Tarun Mangla and Chirag Jain for being supportive like elder brothers. Finally, I would also like to acknowledge special thanks to my parents and sister for always supporting me in my endeavors.

The author also acknowledges the support for this work offered by National Science Foundation under grant award number CAREER-1553212. Any views and conclusions contained herein are those of the author, and do not necessarily represent the official positions, express or implied, of the funders.

TABLE OF CONTENTS

Acknowledgments v

List of Tables viii

List of Figures ix

Summary x

Chapter 1: Introduction 1

Chapter 2: Real-space formulation of Kohn-Sham DFT 4

Chapter 3: Hellmann-Feynman Stress tensor 8

3.1 Stress tensor contribution σ^{T_s} 9

3.2 Stress tensor contribution $\sigma^{E_{xc}}$ 10

3.3 Stress tensor contribution $\sigma^{E_{nl}}$ 11

3.4 Stress tensor contribution $\sigma^{E_{el}}$ 14

3.5 Stress tensor contribution σ^{S} 16

3.6 Stress tensor contribution $\sigma^{\lambda_{mn}}$ 16

3.7 Stress tensor contribution $\sigma^{\lambda_{f}}$ 17

3.8 Total stress tensor 17

Chapter 4: Results and Discussion 20

4.1 Convergence of stress tensor with discretization 21

4.2 Cell optimization using the stress tensor 21

4.3 Stress tensor in ab-initio molecular dynamics 23

Chapter 5: Conclusion 25

Appendices 26

Appendix A: Stress tensor contribution σ^{E_c} 27

Appendix B: On the reformulation of the stress tensor contribution $\sigma^{E_{nl}}$ 29

Appendix C: On the stress tensor contribution $\sigma^{E_{self}}$ in real-space calculations . 30

References 31

LIST OF TABLES

4.1 Computed stress tensor and that obtained from the numerical derivative of the energy for the triclinic titanium system by M-SPARC. All stress component values are reported in GPa. 23

4.2 Stress tensor computed by M-SPARC and ABINIT for the hcp titanium and dc germanium systems. All stress component values are reported in GPa. . . 24

LIST OF FIGURES

2.1 Unit cell Ω (solid blue lines) and its infinitesimally deformed version Ω^F (dashed red lines). The lattice vectors corresponding to Ω are $L_1\hat{\boldsymbol{x}}_{\mathbf{1}}$, $L_2\hat{\boldsymbol{x}}_{\mathbf{2}}$, and $L_3\hat{\boldsymbol{x}}_{\mathbf{3}}$, where $\hat{\boldsymbol{x}}_{\mathbf{1}}$, $\hat{\boldsymbol{x}}_{\mathbf{2}}$, and $\hat{\boldsymbol{x}}_{\mathbf{3}}$ are the lattice unit vectors, with $\theta_1 = \arccos(\hat{\boldsymbol{x}}_{\mathbf{3}}.\hat{\boldsymbol{x}}_{\mathbf{1}})$, $\theta_2 = \arccos(\hat{\boldsymbol{x}}_{\mathbf{2}}.\hat{\boldsymbol{x}}_{\mathbf{3}})$, and $\theta_3 = \arccos(\hat{\boldsymbol{x}}_{\mathbf{1}}.\hat{\boldsymbol{x}}_{\mathbf{2}})$ representing the angles between them. 4

4.1 Convergence of the stress tensor with mesh size for the hcp titanium, triclinic titanium, and dc germanium systems. The error is defined to be magnitude of the maximum difference in any component. The straight lines represent linear fits to the data. 21

4.2 Variation in the energy difference and pressure computed by ABINIT and M-SPARC as a function of volume change for the hcp titanium and dc germanium systems. The volume change and energy difference are defined with respect to the equilibrium system, i.e., cell corresponding to zero stress. 22

B.1 Convergence of the stress tensor with mesh size for the dc germanium system with and without the nonlocal reformulation. The error is defined to be magnitude of the maximum difference in any component. The straight lines represent linear fits to the data. 29

C.1 Convergence of the stress tensor with mesh size for the dc germanium system with and without the contribution arising from the self energy. The error is defined to be magnitude of the maximum difference in any component. The straight lines represent linear fits to the data. 30

SUMMARY

An accurate and efficient formulation of the stress tensor for real-space Kohn-Sham Density Functional Theory (DFT) calculations is presented. Specifically, while employing a local formulation of the electrostatics, a linear-scaling expression for the stress tensor that is applicable to simulations with unit cells of arbitrary symmetry, semilocal exchange-correlation functionals, and Brillouin zone integration is discussed. In particular, the contributions arising from the self energy and the nonlocal pseudopotential energy are rewritten to make them suitable for the real-space finite-difference discretization, achieving up to three orders of magnitude improvement in the accuracy of the computed stresses. Through selected examples representative of static calculations, the accuracy and efficiency of the proposed formulation is verified. In particular, high rates of convergence with spatial discretization, consistency between the computed energy and stress tensor, and very good agreement with reference planewave results are demonstrated.

CHAPTER 1
INTRODUCTION

Kohn-Sham Density Functional Theory (KS-DFT) [1, 2] is an ab-initio method, widely used for understanding and predicting a wide range of material properties. One of the most popular choice of DFT implementation is the expansion of the Kohn-Sham equations in the plane-wave basis [3, 4, 5, 6, 7, 8]. Although, it has many attractive features, yet it suffers from a number of limitations, including its nonlocal nature which severely limits its efficiency in the context of scalable high-performance computing and makes the development of methods that scale linearly with respect to the number of atoms impractical [9, 10]. This has motivated the development of the real-space approaches for DFT, the most popular among which is the finite-difference method [11, 12, 13, 14, 15, 16], wherein the equations are discretized using high-order central finite-differences. These approaches not only overcome the limitations of their plane-wave counterpart, but also achieve speedups of up to an order of magnitude in some cases [16, 15, 17]. Furthermore, the main computational bottleneck of the real-space DFT calculation in a non-orthogonal crystal system, i.e., Laplacian-vector multiplication, has been recently overcome [18, 19], which further makes the real-space method a preferred choice for the ab-initio electronic structure calculations.

One of the key components of DFT calculation is solving the non-linear eigenvalue problem self-consistently, which gives the ground state electron density and energy upon convergence. Once the ground state is determined, the Hellmann-Feynman atomic force [20] can be obtained by taking the derivative of the ground state energy with respect to the atomic coordinates as shown in the previous works [16, 15]. Besides calculating atomic forces, it is often required to calculate the stress (derivative of the ground state energy with respect to the strain) in periodic systems to determine equilibrium lattice constants of the

system, obtain bulk modulus, extract statistical properties from MD simulations like shear viscosity, equation of state and so on. In principle, the stress can be obtained by taking the derivative of the curve fit obtained from the plot of ground state energies at different cell geometries. However, in practice, it is computationally expensive, intractable for large systems and prone to large numerical errors. This motivates the direct calculation of the stress which is the focus of the current work.

In the past, there have been significant efforts to calculate pressure and stress in the periodic systems. Slater et al. [21] gave the expression of pressure for the $X\alpha$ all-electron theory which was later extended to any treatment of exchange and correlation within the muffin-tin approximation by Janak et al. [22]. Yin et al. [23] derived the pressure for the pseudopotential DFT formalism and implemented it using the plane-wave basis. However, the first implementation of the stress tensor in a DFT framework was done by Nielsen and Martin [24, 25] by employing the plane-wave basis expansion and the local-density approximation, which was later extended to the generalized-gradient approximation by Corso et al. [26]. Besides plane-wave based approaches, the stress was derived for a number of other DFT formulations. Thonhauser et al. [27] derived the stress within the linearized augmented plane wave method accounting for the Pulay terms arising due to the dependence of basis functions on the strain. The stress tensor for the projector augmented-wave method [28] also has some additional terms due to the compensating charges of the PAW method. Similarly, Kudin et al. [29] discussed the real space evaluation of the coulomb contribution to the stress tensor for Gaussian-type orbitals using a fast multipole method. Furthermore, the stress calculation in the numeric atom-centered orbital based density-functional formulation is provided for both pseudopotential [30] as well as all-electron [31] calculations. Recently, the configurational force approach [32] is proposed for the calculation of the stress in the context of finite-element discretization, wherein the integrals of Eshelby tensors are calculated.

In this thesis, a real-space formulation of stress in a periodic system of any arbitrary symmetry, particularly suitable for the implementation involving the finite-difference discretization of the underlying Kohn-Sham equations is presented. Essentially, the derivative of the free energy in KS-DFT with respect to the deformation gradient at the ground state of the system is derived. Unlike, the scaling argument used in many previous stress derivations described above, this derivation utilizes the variational nature of the Kohn-Sham DFT and is free from Pulay correction terms arising due to the change in basis functions under strain. Specifically, utilizing a local reformulation of the electrostatics and a reformulation of the non-local pseudopotential component of stress, the stress expression within the generalized gradient approximation is derived and the accuracy and efficiency of the proposed stress formulation is demonstrated through selected examples. This work has been reported in The Journal of Chemical Physics [33] and its extension to $\mathcal{O}(N)$ has been reported in the context of the Spectral Quadrature method [34] in [35].

CHAPTER 2

REAL-SPACE FORMULATION OF KOHN-SHAM DFT

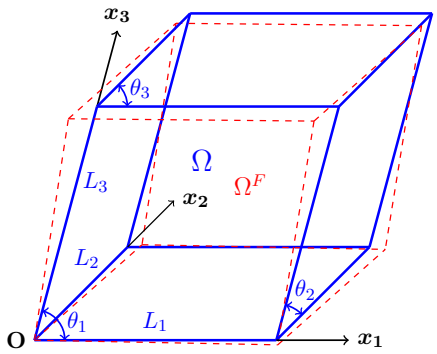

Figure 2.1: Unit cell Ω (solid blue lines) and its infinitesimally deformed version Ω^F (dashed red lines). The lattice vectors corresponding to Ω are $L_1\hat{\boldsymbol{x}}_{\mathbf{1}}$, $L_2\hat{\boldsymbol{x}}_{\mathbf{2}}$, and $L_3\hat{\boldsymbol{x}}_{\mathbf{3}}$, where $\hat{\boldsymbol{x}}_{\mathbf{1}}$, $\hat{\boldsymbol{x}}_{\mathbf{2}}$, and $\hat{\boldsymbol{x}}_{\mathbf{3}}$ are the lattice unit vectors, with $\theta_1 = \arccos(\hat{\boldsymbol{x}}_{\mathbf{3}}.\hat{\boldsymbol{x}}_{\mathbf{1}})$, $\theta_2 = \arccos(\hat{\boldsymbol{x}}_{\mathbf{2}}.\hat{\boldsymbol{x}}_{\mathbf{3}})$, and $\theta_3 = \arccos(\hat{\boldsymbol{x}}_{\mathbf{1}}.\hat{\boldsymbol{x}}_{\mathbf{2}})$ representing the angles between them.

Consider a unit cell Ω as shown in Figure 2.1 with lattice vectors $L_1\hat{\boldsymbol{x}}_{\mathbf{1}}$, $L_2\hat{\boldsymbol{x}}_{\mathbf{2}}$, and $L_3\hat{\boldsymbol{x}}_{\mathbf{3}}$, where $\hat{\boldsymbol{x}}_{\mathbf{1}}$, $\hat{\boldsymbol{x}}_{\mathbf{2}}$, and $\hat{\boldsymbol{x}}_{\mathbf{3}}$ are the lattice unit vectors that are related to the Cartesian unit vectors $\hat{\boldsymbol{e}}_{\mathbf{1}}$, $\hat{\boldsymbol{e}}_{\mathbf{2}}$, and $\hat{\boldsymbol{e}}_{\mathbf{3}}$ via the matrix $\mathbf{S}$, i.e., $\begin{bmatrix}\hat{\boldsymbol{x}}_{\mathbf{1}} & \hat{\boldsymbol{x}}_{\mathbf{2}} & \hat{\boldsymbol{x}}_{\mathbf{3}}\end{bmatrix}^{\mathrm{T}} = \mathbf{S}\begin{bmatrix}\hat{\boldsymbol{e}}_{\mathbf{1}} & \hat{\boldsymbol{e}}_{\mathbf{2}} & \hat{\boldsymbol{e}}_{\mathbf{3}}\end{bmatrix}^{\mathrm{T}}$. In this unit cell, let the nuclei be positioned at $\mathbf{R} = \{\mathbf{R}_1, \mathbf{R}_2, \ldots, \mathbf{R}_N\}$ and contain a total of N_e valence electrons. Neglecting spin and using the pseudopotential approximation, the free energy of the system in Kohn-Sham DFT [1, 2] at finite electronic temperature [36] can be written as

$$\mathcal{F}(\boldsymbol{\Psi}, \mathbf{g}, \phi, \mathbf{R}) = T_s(\boldsymbol{\Psi}, \mathbf{g}) + E_{xc}(\rho, \boldsymbol{\nabla}\rho) + E_{nl}(\boldsymbol{\Psi}, \mathbf{g}, \mathbf{R}) + E_{el}(\rho, \phi, \mathbf{R}) - S(\mathbf{g})\,, \quad (2.1)$$

where T_s is the electronic kinetic energy, E_{xc} is the exchange-correlation energy, E_{nl} is the nonlocal pseudopotential energy, E_{el} is the total electrostatic energy, S is the electronic entropy energy, $\boldsymbol{\Psi} = \{\psi_1, \psi_2, \ldots, \psi_{N_s}\}$ is the collection of orbitals with occupations $\mathbf{g} =$

$\{g_1, g_2, \ldots g_{N_s}\}$, ϕ is the electrostatic potential [37, 38], and ρ is the electron density:

$$\rho(\mathbf{x}) = 2\sum_{n=1}^{N_s} \fint_{BZ} g_n(\mathbf{k}) |\psi_n(\mathbf{x}, \mathbf{k})|^2 \, \mathrm{d}\mathbf{k} \,. \tag{2.2}$$

Above, $\mathbf{k}$ denotes the wavevector and $\fint_{BZ}$ represents the volume average over the Brillouin zone.

The electronic kinetic energy is of the form

$$T_s(\mathbf{\Psi}, \mathbf{g}) = -\sum_{n=1}^{N_s} \fint_{BZ} \int_{\Omega} g_n(\mathbf{k}) \psi_n^*(\mathbf{x}, \mathbf{k}) \nabla^2 \psi_n(\mathbf{x}, \mathbf{k}) \, \mathrm{d}\mathbf{x} \, \mathrm{d}\mathbf{k} \,, \tag{2.3}$$

where ψ_n^* denotes the complex conjugate of ψ_n and $\nabla^2 = \boldsymbol{\nabla}^{\mathrm{T}} \boldsymbol{\nabla}$, with $\boldsymbol{\nabla} = \mathbf{S}^{\text{-}1} \big[\frac{\partial}{\partial x_1} \quad \frac{\partial}{\partial x_2} \quad \frac{\partial}{\partial x_3} \big]^{\mathrm{T}}$ being the gradient defined in the Cartesian coordinate system. The exchange-correlation energy within the semilocal generalized gradient approximation (GGA) [39, 40] can be expressed as

$$E_{xc}(\rho, \boldsymbol{\nabla}\rho) = \int_{\Omega} \varepsilon_{xc}\big(\rho(\mathbf{x}), \boldsymbol{\nabla}\rho(\mathbf{x})\big) \rho(\mathbf{x}) \, \mathrm{d}\mathbf{x} \,, \tag{2.4}$$

where $\varepsilon_{xc} = \varepsilon_x + \varepsilon_c$ is the sum of the exchange and correlation per particle of a uniform electron gas. The nonlocal pseudopotential energy within the Kleinman-Bylander [41] representation takes the form

$$E_{nl}(\mathbf{\Psi}, \mathbf{g}, \mathbf{R}) = 2\sum_{n=1}^{N_s} \fint_{BZ} g_n(\mathbf{k}) \sum_{J} \sum_{lm} \gamma_{\mathrm{Jl}} \left| \int_{\Omega} \tilde{\chi}^*_{\mathrm{Jlm}}(\mathbf{x}, \mathbf{R}_{\mathrm{J}}, \mathbf{k}) \psi_n(\mathbf{x}, \mathbf{k}) \, \mathrm{d}\mathbf{x} \right|^2 \mathrm{d}\mathbf{k} \,, \tag{2.5}$$

where the summation index J runs over all atoms in Ω, lm runs over all azimuthal and magnetic quantum numbers, γ_{Jl} is a normalization constant, and $\tilde{\chi}_{\mathrm{Jlm}}$ are the Bloch-periodically mapped projectors, i.e., $\tilde{\chi}_{\mathrm{Jlm}} = \sum_{J'} \chi_{\mathrm{J'lm}} \, e^{-i\mathbf{k}\cdot(\mathbf{R}_{\mathrm{J}} - \mathbf{R}_{\mathrm{J'}})}$. Here, the summation index J' runs over the J^{th} atom and its periodic images, $\chi_{\mathrm{J'lm}}$ is the corresponding projector, and $i = \sqrt{-1}$. The total electrostatic energy—locally reformulated [42, 43], thus making it

suitable for real-space calculations—can be written as

$$E_{el}(\rho,\phi,\mathbf{R}) = -\frac{1}{8\pi}\int_{\Omega} |\boldsymbol{\nabla}\phi(\mathbf{x})|^2\,\mathrm{d}\mathbf{x} + \int_{\Omega}\big(\rho(\mathbf{x})+b(\mathbf{x},\mathbf{R})\big)\phi(\mathbf{x})\,\mathrm{d}\mathbf{x} - E_{self}(\mathbf{R}) + E_c(\mathbf{R})\,, \tag{2.6}$$

where $b = \sum_I b_I$ represents the total pseudocharge density of the nuclei, with b_I being the pseudocharge density of the I^{th} nucleus and the summation index I running over all atoms in $\mathbb{R}^3$; $E_{self}(\mathbf{R}) = \frac{1}{2}\sum_I \int_\Omega b_I(\mathbf{x},\mathbf{R}_I)V_I(\mathbf{x},\mathbf{R}_I)\,\mathrm{d}\mathbf{x}$ is the self energy associated with the pseudocharge densities, with V_I being the pseudopotential of the I^{th} nucleus and the summation index I again running over all atoms in $\mathbb{R}^3$; and E_c corrects for the error in the repulsive energy when there is overlap of the pseudocharge densities, as discussed in Appendix A. The electronic entropy energy arising due to the partial occupation of orbitals takes the form

$$S(\mathbf{g}) = -2\sigma\sum_{n=1}^{N_s} \fint_{BZ} \Big(g_n(\mathbf{k})\log g_n(\mathbf{k}) + \big(1-g_n(\mathbf{k})\big)\log\big(1-g_n(\mathbf{k})\big)\Big)\,\mathrm{d}\mathbf{k}\,, \tag{2.7}$$

where σ is the electronic smearing.

The electronic ground state for a fixed position of nuclei then is given by the solution of the constrained minimization problem [38, 16]

$$\min_{\boldsymbol{\Psi},\mathbf{g}}\max_{\phi}\mathcal{F}(\boldsymbol{\Psi},\mathbf{g},\phi,\mathbf{R}) \text{ s.t. } \int_\Omega \psi_m^*(\mathbf{x},\mathbf{k})\psi_n(\mathbf{x},\mathbf{k})\,\mathrm{d}\mathbf{x} = \delta_{mn}\ \forall\ \mathbf{k} \quad \text{and} \quad 2\sum_{n=1}^{N_s}\fint_{BZ} g_n(\mathbf{k})\,\mathrm{d}\mathbf{k} = N_e \tag{2.8}$$

where δ_{mn} is the Kronecker delta function. In this variational problem, the functional is minimized over the Bloch-periodic functions defined by: $\psi_n(\mathbf{x}+\mathbf{L},\mathbf{k}) = e^{i\mathbf{k}.\mathbf{L}}\psi_n(\mathbf{x},\mathbf{k})$ for every lattice vector $\mathbf{L}$ and Bloch wavevector $\mathbf{k}$. The corresponding Euler-Lagrange equations take the form:

$$\left(\mathcal{H} \equiv -\frac{1}{2}\nabla^2 + V_{xc} + \phi + V_{nl}\right)\psi_n \quad = \quad \lambda_n\psi_n\,, \quad n = 1,2,\ldots,N_s\,, \tag{2.9}$$

$$g_n(\mathbf{k}) = \left(1 + \exp\left(\frac{\lambda_n(\mathbf{k}) - \lambda_f}{\sigma}\right)\right)^{-1}, \lambda_f \quad \text{is s.t.} \quad 2\sum_{n=1}^{N_s} \fint_{BZ} g_n(\mathbf{k})\,\mathrm{d}\mathbf{k} = N_e \tag{2.10}$$

$$-\frac{1}{4\pi}\nabla^2\phi(\mathbf{x},\mathbf{R}) \quad = \quad \rho(\mathbf{x}) + b(\mathbf{x},\mathbf{R})\,, \tag{2.11}$$

where $\mathcal{H}$ is the Hamiltonian with eigenfunctions ψ_n and eigenvalues λ_n, λ_f is the Fermi level, V_{xc} is the exchange-correlation potential:

$$V_{xc} = \frac{\delta E_{xc}}{\delta\rho} = \varepsilon_{xc} + \rho\frac{\partial\varepsilon_{xc}}{\partial\rho} - \boldsymbol{\nabla}\cdot\left(\rho\frac{\partial\varepsilon_{xc}}{\partial(\boldsymbol{\nabla}\rho)}\right)\,, \tag{2.12}$$

and V_{nl} is the nonlocal pseudopotential operator:

$$V_{nl}\psi_n = \sum_J \sum_{lm} \gamma_{\mathrm{Jl}}\tilde{\chi}_{\mathrm{Jlm}}\left(\int_\Omega \tilde{\chi}^*_{\mathrm{Jlm}}(\mathbf{x},\mathbf{R}_\mathbf{J},\mathbf{k})\psi_n(\mathbf{x},\mathbf{k})\,\mathrm{d}\mathbf{x}\right)\,. \tag{2.13}$$

Once the electronic ground state has been determined, the Hellmann-Feynman stress tensor can be calculated, the expression for which we derive in the next chapter.

CHAPTER 3

HELLMANN-FEYNMAN STRESS TENSOR

Consider an infinitesimal homogeneous deformation that maps the unit cell Ω to Ω^F, as shown in Figure 2.1. Using $\mathbf{F}$ to denote the deformation gradient in Cartesian coordinates, the stress tensor can be defined as

$$\boldsymbol{\sigma}_{\alpha\beta} = \frac{1}{|\Omega|} \frac{\partial \mathcal{L}^F(\boldsymbol{\Psi}, \mathbf{g}, \phi, \mathbf{R}^F)}{\partial \mathbf{F}_{\alpha\beta}} \bigg|_{\mathcal{G}}, \quad \alpha, \beta \in \{1, 2, 3\}, \tag{3.1}$$

where $|\Omega|$ is the measure of the unit cell [1], the superscript $(.)^F$ is used to denote quantities after deformation—a notation adopted henceforth, $\mathcal{G}$ signifies the electronic ground state corresponding to the undeformed unit cell Ω, i.e., at $\mathbf{F} = \mathbf{I}$, and the Lagrangian

$$\begin{aligned} \mathcal{L}^F(\boldsymbol{\Psi}, \mathbf{g}, \phi, \mathbf{R}^F) &= \mathcal{F}^F(\boldsymbol{\Psi}, \mathbf{g}, \phi, \mathbf{R}^F) - 2 \sum_{mn} \fint_{BZ^F} \lambda_{mn}(\mathbf{k}^F) \Bigg(\int_{\Omega^F} \psi_m^*(\mathbf{x}^F, \mathbf{k}^F) \psi_n(\mathbf{x}^F, \mathbf{k}^F) \, \mathrm{d}\mathbf{x}^{\mathrm{F}} \\ &- \delta_{mn} \Bigg) \mathrm{d}\mathbf{k}^{\mathrm{F}} - \lambda_f \left(2 \sum_{n=1}^{N_s} \fint_{BZ^F} \mathrm{g}_n(\mathbf{k}^F) \, \mathrm{d}\mathbf{k}^{\mathrm{F}} - N_e \right). \end{aligned} \tag{3.2}$$

Here, λ_f and $\lambda_{mn} (m, n = 1, 2, \cdots N_s)$ are the Lagrange multipliers used to enforce the constraint on the total number of electrons and the orthonormality of the orbitals, respectively. Note that the above mentioned quantum mechanical stress tensor has resemblance to the Cauchy stress tensor widely used in continuum mechanics.

In Sections section 3.1- section 3.7 below, we derive the contributions to the stress tensor arising from the various terms in $\mathcal{L}^F$, before presenting the expression for the total stress in Section section 3.8. In so doing, we will use a hat $\hat{(.)}$ to denote all ground state quantities, $\det(\mathbf{F})$ to denote the determinant of the matrix $\mathbf{F}$, and $\boldsymbol{\nabla}_\alpha$ ($\alpha \in 1, 2, 3$) to denote

[1] The measure of the unit cell is its volume, area, and length for systems that are extended in three, two, and one dimensions, respectively.

the α^{th} component of the gradient vector. In addition, we will use the relations:

$$\mathbf{x}^F = \mathbf{Q}\mathbf{x}\,, \quad \mathbf{R}^F = \mathbf{Q}\mathbf{R}\,, \quad \mathbf{k}^F = \mathbf{Q}^{-\mathrm{T}}\mathbf{k}\,, \quad \mathbf{F}^{-1} \approx 2 - \mathbf{F}\,, \tag{3.3}$$

where $\mathbf{Q} = \mathbf{S}^{-\mathrm{T}}\mathbf{F}\mathbf{S}^{\mathrm{T}}$. The final relation is a consequence of the deformation being infinitesimal in nature.

3.1 Stress tensor contribution σ^{T_s}

The contribution to the stress tensor arising from the electronic kinetic energy:

$$\begin{aligned}
\sigma^{T_s}_{\alpha\beta} &= \left.\frac{\partial T_s^F(\boldsymbol{\Psi}, \mathbf{g})}{\partial \mathbf{F}_{\alpha\beta}}\right|_{\mathcal{G}} \\
&= \frac{\partial}{\partial \mathbf{F}_{\alpha\beta}}\left(-\sum_{n=1}^{N_s} \fint_{BZ^F} \int_{\Omega^F} g_n(\mathbf{k}^F)\psi_n^*(\mathbf{x}^F, \mathbf{k}^F)\nabla^2\psi_n(\mathbf{x}^F, \mathbf{k}^F)\,\mathrm{d}\mathbf{x}^{\mathrm{F}}\,\mathrm{d}\mathbf{k}^{\mathrm{F}}\right)\Bigg|_{\mathcal{G}} \\
&= \frac{\partial}{\partial \mathbf{F}_{\alpha\beta}}\Bigg(-\sum_{n=1}^{N_s} \fint_{BZ} \int_{\Omega} g_n(\mathbf{Q}^{-\mathrm{T}}\mathbf{k})\psi_n^*(\mathbf{Q}\mathbf{x}, \mathbf{Q}^{-\mathrm{T}}\mathbf{k})\big[\boldsymbol{\nabla}^{\mathrm{T}}\mathbf{F}^{\text{-}1}\mathbf{F}^{\text{-}\mathrm{T}}\boldsymbol{\nabla}\big]\psi_n(\mathbf{Q}\mathbf{x}, \mathbf{Q}^{-\mathrm{T}}\mathbf{k}) \\
&\times \det(\mathbf{F})\,\mathrm{d}\mathbf{x}\,\mathrm{d}\mathbf{k}\Bigg)\Bigg|_{\mathcal{G}} \\
&= A_1 + A_2 + A_3 + A_4 + A_5\,,
\end{aligned} \tag{3.4}$$

where

$$\begin{aligned}
A_1 &= -\sum_{n=1}^{N_s} \fint_{BZ} \int_{\Omega} \left.\frac{\partial g_n(\mathbf{Q}^{-\mathrm{T}}\mathbf{k})}{\partial \mathbf{F}_{\alpha\beta}}\right|_{\mathcal{G}} \hat{\psi}_n^*(\mathbf{x}, \mathbf{k})\nabla^2\hat{\psi}_n(\mathbf{x}, \mathbf{k})\,\mathrm{d}\mathbf{x}\,\mathrm{d}\mathbf{k}\,, \\
A_2 &= -\sum_{n=1}^{N_s} \fint_{BZ} \int_{\Omega} \hat{\mathrm{g}}_n(\mathbf{k}) \left.\frac{\partial \psi_n^*(\mathbf{Q}\mathbf{x}, \mathbf{Q}^{-\mathrm{T}}\mathbf{k})}{\partial \mathbf{F}_{\alpha\beta}}\right|_{\mathcal{G}} \nabla^2\hat{\psi}_n(\mathbf{x}, \mathbf{k})\,\mathrm{d}\mathbf{x}\,\mathrm{d}\mathbf{k}\,, \\
A_3 &= -\sum_{n=1}^{N_s} \fint_{BZ} \int_{\Omega} \hat{\mathrm{g}}_n(\mathbf{k})\hat{\psi}_n^*(\mathbf{x}, \mathbf{k})\nabla^2 \left.\frac{\partial \psi_n(\mathbf{Q}\mathbf{x}, \mathbf{Q}^{-\mathrm{T}}\mathbf{k})}{\partial \mathbf{F}_{\alpha\beta}}\right|_{\mathcal{G}} \mathrm{d}\mathbf{x}\,\mathrm{d}\mathbf{k}\,, \\
A_4 &= -\sum_{n=1}^{N_s} \fint_{BZ} \int_{\Omega} \hat{\mathrm{g}}_n(\mathbf{k})\hat{\psi}_n^*(\mathbf{x}, \mathbf{k})\nabla^2\hat{\psi}_n(\mathbf{x}, \mathbf{k}) \left.\frac{\partial\big(\det(\mathbf{F})\big)}{\partial \mathbf{F}_{\alpha\beta}}\right|_{\mathcal{G}} \mathrm{d}\mathbf{x}\,\mathrm{d}\mathbf{k}
\end{aligned}$$

$$
\begin{aligned}
&= -\sum_{n=1}^{N_s} \fint_{BZ} \int_{\Omega} \hat{\mathbf{g}}_n(\mathbf{k}) \hat{\psi}_n^*(\mathbf{x},\mathbf{k}) \nabla^2 \hat{\psi}_n(\mathbf{x},\mathbf{k}) \delta_{\alpha\beta} \,\mathrm{d}\mathbf{x}\,\mathrm{d}\mathbf{k}\,, \\
A_5 &= -\sum_{n=1}^{N_s} \fint_{BZ} \int_{\Omega} \hat{\mathbf{g}}_n(\mathbf{k}) \hat{\psi}_n^*(\mathbf{x},\mathbf{k}) \frac{\partial\big(\boldsymbol{\nabla}^{\mathrm{T}} \mathbf{F}^{\text{-}1} \mathbf{F}^{\text{-}\mathrm{T}} \boldsymbol{\nabla}\big)}{\partial \mathbf{F}_{\alpha\beta}}\bigg|_{\mathcal{G}} \hat{\psi}_n(\mathbf{x},\mathbf{k}) \,\mathrm{d}\mathbf{x}\,\mathrm{d}\mathbf{k} \\
&= -\sum_{n=1}^{N_s} \fint_{BZ} \int_{\Omega} \hat{\mathbf{g}}_n(\mathbf{k}) \hat{\psi}_n^*(\mathbf{x},\mathbf{k}) \big[-\boldsymbol{\nabla}_\alpha \boldsymbol{\nabla}_\beta - \boldsymbol{\nabla}_\beta \boldsymbol{\nabla}_\alpha\big] \hat{\psi}_n(\mathbf{x},\mathbf{k}) \,\mathrm{d}\mathbf{x}\,\mathrm{d}\mathbf{k} \\
&= -2 \sum_{n=1}^{N_s} \fint_{BZ} \int_{\Omega} \hat{\mathbf{g}}_n(\mathbf{k}) \boldsymbol{\nabla}_\alpha \hat{\psi}_n^*(\mathbf{x},\mathbf{k}) \boldsymbol{\nabla}_\beta \hat{\psi}_n(\mathbf{x},\mathbf{k}) \,\mathrm{d}\mathbf{x}\,\mathrm{d}\mathbf{k}\,.
\end{aligned}
$$

The last equality in A_5 is obtained via integration by parts, performed to reduce the number of derivative evaluations and circumvent the need for mixed derivatives, which are typically more costly to evaluate within the real-space method [19, 18].

3.2 Stress tensor contribution $\sigma^{E_{xc}}$

The contribution to the stress tensor arising from the exchange-correlation energy:

$$
\begin{aligned}
\sigma_{\alpha\beta}^{E_{xc}} &= \frac{\partial E_{xc}^F(\rho, \boldsymbol{\nabla}\rho)}{\partial \mathbf{F}_{\alpha\beta}}\bigg|_{\mathcal{G}} \\
&= \frac{\partial}{\partial \mathbf{F}_{\alpha\beta}} \left(\int_{\Omega^F} \varepsilon_{xc}\big(\rho(\mathbf{x}^F), \boldsymbol{\nabla}\rho(\mathbf{x}^F)\big) \rho(\mathbf{x}^F) \,\mathrm{d}\mathbf{x}^{\mathrm{F}} \right)\bigg|_{\mathcal{G}} \\
&= \frac{\partial}{\partial \mathbf{F}_{\alpha\beta}} \left(\int_{\Omega} \varepsilon_{xc}\big(\rho(\mathbf{Q}\mathbf{x}), \mathbf{F}^{\text{-}\mathrm{T}} \boldsymbol{\nabla}\rho(\mathbf{Q}\mathbf{x})\big) \rho(\mathbf{Q}\mathbf{x}) \det(\mathbf{F}) \,\mathrm{d}\mathbf{x} \right)\bigg|_{\mathcal{G}} \\
&= B_1 + B_2 + B_3 + B_4 + B_5\,, \qquad (3.5)
\end{aligned}
$$

where

$$
\begin{aligned}
B_1 &= 2 \sum_{n=1}^{N_s} \fint_{BZ} \int_{\Omega} V_{xc}\big(\hat{\rho}(\mathbf{x}), \boldsymbol{\nabla}\hat{\rho}(\mathbf{x})\big) \frac{\partial g_n(\mathbf{Q}^{-\mathrm{T}}\mathbf{k})}{\partial \mathbf{F}_{\alpha\beta}}\bigg|_{\mathcal{G}} \big|\hat{\psi}_n(\mathbf{x},\mathbf{k})\big|^2 \,\mathrm{d}\mathbf{x}\,, \\
B_2 &= 2 \sum_{n=1}^{N_s} \fint_{BZ} \int_{\Omega} V_{xc}\big(\hat{\rho}(\mathbf{x}), \boldsymbol{\nabla}\hat{\rho}(\mathbf{x})\big) \hat{\mathbf{g}}_n(\mathbf{k}) \frac{\partial \psi_n^*(\mathbf{Q}\mathbf{x}, \mathbf{Q}^{-\mathrm{T}}\mathbf{k})}{\partial \mathbf{F}_{\alpha\beta}}\bigg|_{\mathcal{G}} \hat{\psi}_n(\mathbf{x},\mathbf{k}) \,\mathrm{d}\mathbf{x}\,, \\
B_3 &= 2 \sum_{n=1}^{N_s} \fint_{BZ} \int_{\Omega} V_{xc}\big(\hat{\rho}(\mathbf{x}), \boldsymbol{\nabla}\hat{\rho}(\mathbf{x})\big) \hat{\mathbf{g}}_n(\mathbf{k}) \hat{\psi}_n^*(\mathbf{x},\mathbf{k}) \frac{\partial \psi_n(\mathbf{Q}\mathbf{x}, \mathbf{Q}^{-\mathrm{T}}\mathbf{k})}{\partial \mathbf{F}_{\alpha\beta}}\bigg|_{\mathcal{G}} \,\mathrm{d}\mathbf{x}\,,
\end{aligned}
$$

$$
\begin{aligned}
B_4 &= \int_\Omega \varepsilon_{xc}\big(\hat\rho(\mathbf{x}), \boldsymbol{\nabla}\hat\rho(\mathbf{x})\big)\hat\rho(\mathbf{x})\frac{\partial\big(\det(\mathbf{F})\big)}{\partial \mathbf{F}_{\alpha\beta}}\bigg|_{\mathcal{G}} \mathrm{d}\mathbf{x} \\
&= \int_\Omega \varepsilon_{xc}\big(\hat\rho(\mathbf{x}), \boldsymbol{\nabla}\hat\rho(\mathbf{x})\big)\hat\rho(\mathbf{x})\delta_{\alpha\beta}\,\mathrm{d}\mathbf{x} \\
&= \delta_{\alpha\beta}E_{xc}(\hat\rho, \boldsymbol{\nabla}\hat\rho)\,, \\
B_5 &= \int_\Omega \hat\rho(\mathbf{x})\frac{\partial\varepsilon_{xc}\big(\hat\rho(\mathbf{x}), \boldsymbol{\nabla}\hat\rho(\mathbf{x})\big)}{\partial\big(\boldsymbol{\nabla}\hat\rho(\mathbf{x})\big)}\frac{\partial \mathbf{F}^{-\mathrm{T}}}{\partial \mathbf{F}_{\alpha\beta}}\bigg|_{\mathcal{G}} \boldsymbol{\nabla}\hat\rho(\mathbf{x})\,\mathrm{d}\mathbf{x} \\
&= -\int_\Omega \hat\rho(\mathbf{x})\frac{\partial\varepsilon_{xc}\big(\hat\rho(\mathbf{x}), \boldsymbol{\nabla}\hat\rho(\mathbf{x})\big)}{\partial\big(\boldsymbol{\nabla}_\beta\hat\rho(\mathbf{x})\big)}\boldsymbol{\nabla}_\alpha\hat\rho(\mathbf{x})\,\mathrm{d}\mathbf{x}\,.
\end{aligned}
$$

In obtaining the terms B_1, B_2, and B_3, we have used the relation:

$$
\begin{aligned}
\frac{\partial\rho(\mathbf{Q}\mathbf{x})}{\partial \mathbf{F}_{\alpha\beta}} &= 2\sum_{n=1}^{N_s}\fint_{BZ}\Bigg(\frac{\partial g_n(\mathbf{Q}^{-\mathrm{T}}\mathbf{x})}{\partial \mathbf{F}_{\alpha\beta}}\left|\psi_n(\mathbf{Q}\mathbf{x}, \mathbf{Q}^{-\mathrm{T}}\mathbf{k})\right|^2 + g_n(\mathbf{Q}^{-\mathrm{T}}\mathbf{k})\frac{\partial\psi_n^*(\mathbf{Q}\mathbf{x}, \mathbf{Q}^{-\mathrm{T}}\mathbf{k})}{\partial \mathbf{F}_{\alpha\beta}} \\
&\times\ \psi_n(\mathbf{Q}\mathbf{x}, \mathbf{Q}^{-\mathrm{T}}\mathbf{k}) + g_n(\mathbf{Q}^{-\mathrm{T}}\mathbf{k})\psi_n^*(\mathbf{Q}\mathbf{x}, \mathbf{Q}^{-\mathrm{T}}\mathbf{k})\frac{\partial\psi_n(\mathbf{Q}\mathbf{x}, \mathbf{Q}^{-\mathrm{T}}\mathbf{k})}{\partial \mathbf{F}_{\alpha\beta}}\Bigg)\,\mathrm{d}\mathbf{k}\,. \quad (3.6)
\end{aligned}
$$

3.3 Stress tensor contribution $\sigma^{E_{nl}}$

The contribution to the stress tensor arising from the nonlocal pseudopotential energy:

$$
\begin{aligned}
\sigma_{\alpha\beta}^{E_{nl}} &= \frac{\partial E_{nl}^F(\boldsymbol{\Psi}, \mathbf{g}, \mathbf{R}^F)}{\partial \mathbf{F}_{\alpha\beta}}\bigg|_{\mathcal{G}} \\
&= \frac{\partial}{\partial \mathbf{F}_{\alpha\beta}}\Bigg(2\sum_{n=1}^{N_s}\fint_{BZ^F} g_n(\mathbf{k}^F)\sum_J\sum_{lm}\gamma_{\mathrm{Jl}}\left|\int_{\Omega^F}\tilde\chi_{\mathrm{Jlm}}^*(\mathbf{x}^F, \mathbf{R}_J^F, \mathbf{k}^F)\psi_n(\mathbf{x}^F, \mathbf{k}^F)\,\mathrm{d}\mathbf{x}^{\mathrm{F}}\right|^2\mathrm{d}\mathbf{k}^{\mathrm{F}}\Bigg)\bigg|_{\mathcal{G}} \\
&= \frac{\partial}{\partial \mathbf{F}_{\alpha\beta}}\Bigg(2\sum_{n=1}^{N_s}\fint_{BZ} g_n(\mathbf{Q}^{-\mathrm{T}}\mathbf{k})\sum_J\sum_{lm}\gamma_{\mathrm{Jl}}\left|\int_{\Omega}\tilde\chi_{\mathrm{Jlm}}^*(\mathbf{Q}\mathbf{x}, \mathbf{Q}\mathbf{R}_J, \mathbf{Q}^{-\mathrm{T}}\mathbf{k})\psi_n(\mathbf{Q}\mathbf{x}, \mathbf{Q}^{-\mathrm{T}}\mathbf{k})\right. \\
&\times\ \left.\det(\mathbf{F})\,\mathrm{d}\mathbf{x}\right|^2\mathrm{d}\mathbf{k}\Bigg)\bigg|_{\mathcal{G}} \\
&= C_1 + C_2 + C_3 + C_4 + C_5\,, \quad (3.7)
\end{aligned}
$$

where

$$
\begin{aligned}
C_1 &= 2\sum_{n=1}^{N_s} \fint_{BZ} \frac{\partial g_n(\mathbf{Q}^{-\mathrm{T}}\mathbf{k})}{\partial \mathbf{F}_{\alpha\beta}}\bigg|_{\mathcal{G}} \sum_J \sum_{lm} \gamma_{\mathrm{Jl}} \bigg| \int_\Omega \tilde{\chi}^*_{\mathrm{Jlm}}(\mathbf{x},\mathbf{R}_\mathrm{J},\mathbf{k})\hat{\psi}_n(\mathbf{x},\mathbf{k})\,\mathrm{d}\mathbf{x}\bigg|^2 \mathrm{d}\mathbf{k}\,,\\
C_2 &= 2\sum_{n=1}^{N_s} \fint_{BZ} \hat{\mathbf{g}}_n(\mathbf{k}) \sum_J \sum_{lm} \gamma_{\mathrm{Jl}} \bigg(\int_\Omega \tilde{\chi}^*_{\mathrm{Jlm}}(\mathbf{x},\mathbf{R}_\mathrm{J},\mathbf{k})\hat{\psi}_n(\mathbf{x},\mathbf{k})\,\mathrm{d}\mathbf{x}\bigg)\bigg(\int_\Omega \tilde{\chi}_{\mathrm{Jlm}}(\mathbf{x},\mathbf{R}_\mathrm{J},\mathbf{k})\\
&\times \frac{\partial \psi^*_n(\mathbf{Q}\mathbf{x},\mathbf{Q}^{-\mathrm{T}}\mathbf{k})}{\partial \mathbf{F}_{\alpha\beta}}\bigg|_{\mathcal{G}} \mathrm{d}\mathbf{x}\bigg)\,\mathrm{d}\mathbf{k}\,,\\
C_3 &= 2\sum_{n=1}^{N_s} \fint_{BZ} \hat{\mathbf{g}}_n(\mathbf{k}) \sum_J \sum_{lm} \gamma_{\mathrm{Jl}} \bigg(\int_\Omega \tilde{\chi}^*_{\mathrm{Jlm}}(\mathbf{x},\mathbf{R}_\mathrm{J},\mathbf{k}) \frac{\partial \psi_n(\mathbf{Q}\mathbf{x},\mathbf{Q}^{-\mathrm{T}}\mathbf{k})}{\partial \mathbf{F}_{\alpha\beta}}\bigg|_{\mathcal{G}} \mathrm{d}\mathbf{x}\bigg)\\
&\times \bigg(\int_\Omega \tilde{\chi}_{\mathrm{Jlm}}(\mathbf{x},\mathbf{R}_\mathrm{J},\mathbf{k})\hat{\psi}^*_n(\mathbf{x},\mathbf{k})\,\mathrm{d}\mathbf{x}\bigg)\,\mathrm{d}\mathbf{k}\,,\\
C_4 &= 4\sum_{n=1}^{N_s} \fint_{BZ} \hat{\mathbf{g}}_n(\mathbf{k}) \sum_J \sum_{lm} \gamma_{\mathrm{Jl}} \bigg(\int_\Omega \tilde{\chi}^*_{\mathrm{Jlm}}(\mathbf{x},\mathbf{R}_\mathrm{J},\mathbf{k})\hat{\psi}_n(\mathbf{x},\mathbf{k}) \frac{\partial\big(\det(\mathbf{F})\big)}{\partial \mathbf{F}_{\alpha\beta}}\bigg|_{\mathcal{G}} \mathrm{d}\mathbf{x}\bigg)\\
&\times \bigg(\int_\Omega \tilde{\chi}_{\mathrm{Jlm}}(\mathbf{x},\mathbf{R}_\mathrm{J},\mathbf{k})\hat{\psi}^*_n(\mathbf{x},\mathbf{k})\,\mathrm{d}\mathbf{x}\bigg)\,\mathrm{d}\mathbf{k}\\
&= 4\sum_{n=1}^{N_s} \fint_{BZ} \hat{\mathbf{g}}_n(\mathbf{k}) \sum_J \sum_{lm} \gamma_{\mathrm{Jl}} \int_\Omega \tilde{\chi}^*_{\mathrm{Jlm}}(\mathbf{x},\mathbf{R}_\mathrm{J},\mathbf{k})\hat{\psi}_n(\mathbf{x},\mathbf{k})\delta_{\alpha\beta}\,\mathrm{d}\mathbf{x} \int_\Omega \tilde{\chi}_{\mathrm{Jlm}}(\mathbf{x},\mathbf{R}_\mathrm{J},\mathbf{k})\hat{\psi}^*_n(\mathbf{x},\mathbf{k})\,\mathrm{d}\mathbf{x}\,\mathrm{d}\mathbf{k}\\
&= 2\delta_{\alpha\beta} E_{nl}(\hat{\mathbf{\Psi}},\hat{\mathbf{g}},\mathbf{R})\,,\\
C_5 &= 4\sum_{n=1}^{N_s} \fint_{BZ} \hat{\mathbf{g}}_n(\mathbf{k}) \sum_J \sum_{lm} \gamma_{\mathrm{Jl}} \Re\bigg[\bigg(\int_\Omega \frac{\partial \tilde{\chi}^*_{\mathrm{Jlm}}(\mathbf{Q}\mathbf{x},\mathbf{Q}\mathbf{R}_J,\mathbf{Q}^{-\mathrm{T}}\mathbf{k})}{\partial \mathbf{F}_{\alpha\beta}}\bigg|_{\mathcal{G}} \hat{\psi}_n(\mathbf{x},\mathbf{k})\,\mathrm{d}\mathbf{x}\bigg)\\
&\times \bigg(\int_\Omega \tilde{\chi}_{\mathrm{Jlm}}(\mathbf{x},\mathbf{R}_\mathrm{J},\mathbf{k})\hat{\psi}^*_n(\mathbf{x},\mathbf{k})\,\mathrm{d}\mathbf{x}\bigg)\bigg]\,\mathrm{d}\mathbf{k}\\
&= 4\sum_{n=1}^{N_s} \fint_{BZ} \hat{\mathbf{g}}_n(\mathbf{k}) \sum_J \sum_{lm} \gamma_{\mathrm{Jl}} \Re\bigg[\bigg(\sum_{J'} \int_\Omega \boldsymbol{\nabla}_\alpha \chi^*_{\mathrm{J'lm}}(\mathbf{x},\mathbf{R}_{\mathrm{J'}}) e^{i\mathbf{k}\cdot(\mathbf{R}_\mathrm{J}-\mathbf{R}_{\mathrm{J'}})}\big(\mathbf{S}^{\mathrm{T}}\mathbf{x} - \mathbf{S}^{\mathrm{T}}\mathbf{R}_{\mathrm{J'}}\big)_\beta\\
&\times \hat{\psi}_n(\mathbf{x},\mathbf{k})\,\mathrm{d}\mathbf{x}\bigg)\bigg(\int_\Omega \tilde{\chi}_{\mathrm{Jlm}}(\mathbf{x},\mathbf{R}_\mathrm{J},\mathbf{k})\hat{\psi}^*_n(\mathbf{x},\mathbf{k})\,\mathrm{d}\mathbf{x}\bigg)\bigg]\,\mathrm{d}\mathbf{k}\\
&= -4\sum_{n=1}^{N_s} \fint_{BZ} \hat{\mathbf{g}}_n(\mathbf{k}) \sum_J \sum_{lm} \gamma_{\mathrm{Jl}} \Re\bigg[\bigg(\sum_{J'} \int_\Omega \chi^*_{\mathrm{J'lm}}(\mathbf{x},\mathbf{R}_{\mathrm{J'}}) e^{i\mathbf{k}\cdot(\mathbf{R}_\mathrm{J}-\mathbf{R}_{\mathrm{J'}})}\big(\mathbf{S}^{\mathrm{T}}\mathbf{x} - \mathbf{S}^{\mathrm{T}}\mathbf{R}_{\mathrm{J'}}\big)_\beta\\
&\times \boldsymbol{\nabla}_\alpha \hat{\psi}_n(\mathbf{x},\mathbf{k})\,\mathrm{d}\mathbf{x}\bigg)\bigg(\int_\Omega \tilde{\chi}_{\mathrm{Jlm}}(\mathbf{x},\mathbf{R}_\mathrm{J},\mathbf{k})\hat{\psi}^*_n(\mathbf{x},\mathbf{k})\,\mathrm{d}\mathbf{x}\bigg)\bigg]\,\mathrm{d}\mathbf{k} - 2\delta_{\alpha\beta} E_{nl}(\hat{\mathbf{\Psi}},\hat{\mathbf{g}},\mathbf{R})\,.
\end{aligned}
$$

In deriving the expression for C_5, the second equality is obtained by using the relation:

$$\begin{aligned}
\left.\frac{\partial\tilde{\chi}^{*}_{\mathrm{Jlm}}(\mathbf{Q}\mathbf{x},\mathbf{Q}\mathbf{R}_J,\mathbf{Q}^{-\mathrm{T}}\mathbf{k})}{\partial\mathbf{F}_{\alpha\beta}}\right|_{\mathcal{G}} &= \sum_{J'}\left(\frac{\partial\chi^{*}_{\mathrm{J'lm}}(\mathbf{Q}\mathbf{x},\mathbf{Q}\mathbf{R}_{J'})}{\partial(\mathbf{Q}\mathbf{x})}\frac{\partial(\mathbf{Q}\mathbf{x})}{\partial\mathbf{F}_{\alpha\beta}}+\frac{\partial\chi^{*}_{\mathrm{J'lm}}(\mathbf{Q}\mathbf{x},\mathbf{Q}\mathbf{R}_{J'})}{\partial(\mathbf{Q}\mathbf{R}_{J'})}\frac{\partial(\mathbf{Q}\mathbf{R}_{J'})}{\partial\mathbf{F}_{\alpha\beta}}\right)\Bigg|_{\mathcal{G}} \\
&\times\ e^{i\mathbf{k}\cdot(\mathbf{R}_{\mathrm{J}}-\mathbf{R}_{\mathrm{J'}})} \\
&= \sum_{J'}\left[\boldsymbol{\nabla}_{\alpha}\chi^{*}_{\mathrm{J'lm}}(\mathbf{x},\mathbf{R}_{\mathrm{J'}})\big(\mathbf{S}^{\mathrm{T}}\mathbf{x}\big)_{\beta}+\left(\frac{\partial\chi^{*}_{\mathrm{J'lm}}(\mathbf{x},\mathbf{R}_{\mathrm{J'}})}{\partial\mathbf{R}_{\mathrm{J'}}}\mathbf{S}^{\text{-T}}\right)_{\alpha}\big(\mathbf{S}^{\mathrm{T}}\mathbf{R}_{\mathrm{J'}}\big)_{\beta}\right] \\
&\times\ e^{i\mathbf{k}\cdot(\mathbf{R}_{\mathrm{J}}-\mathbf{R}_{\mathrm{J'}})} \\
&= \sum_{J'}\boldsymbol{\nabla}_{\alpha}\chi^{*}_{\mathrm{J'lm}}(\mathbf{x},\mathbf{R}_{\mathrm{J'}})e^{i\mathbf{k}\cdot(\mathbf{R}_{\mathrm{J}}-\mathbf{R}_{\mathrm{J'}})}\big(\mathbf{S}^{\mathrm{T}}\mathbf{x}-\mathbf{S}^{\mathrm{T}}\mathbf{R}_{\mathrm{J'}}\big)_{\beta}\,, \qquad (3.8)
\end{aligned}$$

where the third equality is obtained by using the relation $\chi^{*}_{\mathrm{J'lm}}(\mathbf{x},\mathbf{R}_{\mathrm{J'}}) = \chi^{*}_{\mathrm{J'lm}}(\mathbf{S}^{\mathrm{T}}\mathbf{x} - \mathbf{S}^{\mathrm{T}}\mathbf{R}_{\mathrm{J'}})$. The third equality in deriving the expression for C_5 is obtained as follows:

$$\begin{aligned}
\chi^{\sigma}_{\alpha\beta} &= \sum_{J'}\int_{\Omega}\boldsymbol{\nabla}_{\alpha}\chi^{*}_{\mathrm{J'lm}}(\mathbf{x},\mathbf{R}_{\mathrm{J'}})e^{i\mathbf{k}\cdot(\mathbf{R}_{\mathrm{J}}-\mathbf{R}_{\mathrm{J'}})}\big(\mathbf{S}^{\mathrm{T}}\mathbf{x}-\mathbf{S}^{\mathrm{T}}\mathbf{R}_{\mathrm{J'}}\big)_{\beta}\hat{\psi}_n(\mathbf{x},\mathbf{k})\,\mathrm{d}\mathbf{x} \\
&= \sum_{J'}\int_{\Omega}\left(\frac{\partial\chi^{*}_{\mathrm{J'lm}}(\mathbf{x},\mathbf{R}_{\mathrm{J'}})}{\partial\mathbf{R}_{\mathrm{J'}}}\mathbf{S}^{\text{-T}}\right)_{\alpha}e^{i\mathbf{k}\cdot(\mathbf{R}_{\mathrm{J}}-\mathbf{R}_{\mathrm{J'}})}\big(\mathbf{S}^{\mathrm{T}}\mathbf{R}_{\mathrm{J'}}-\mathbf{S}^{\mathrm{T}}\mathbf{x}\big)_{\beta}\hat{\psi}_n(\mathbf{x},\mathbf{k})\,\mathrm{d}\mathbf{x} \\
&= \sum_{J'}\int_{\Omega}\left(\frac{\partial}{\partial\mathbf{R}_{\mathrm{J'}}}\mathbf{S}^{\text{-T}}\right)_{\alpha}\left[\chi^{*}_{\mathrm{J'lm}}(\mathbf{x},\mathbf{R}_{\mathrm{J'}})\big(\mathbf{S}^{\mathrm{T}}\mathbf{R}_{\mathrm{J'}}-\mathbf{S}^{\mathrm{T}}\mathbf{x}\big)_{\beta}e^{i\mathbf{k}\cdot(\mathbf{R}_{\mathrm{J}}-\mathbf{R}_{\mathrm{J'}})}\hat{\psi}_n(\mathbf{x},\mathbf{k})\right]\mathrm{d}\mathbf{x} \\
&- \delta_{\alpha\beta}\sum_{J'}\int_{\Omega}\chi^{*}_{\mathrm{J'lm}}(\mathbf{x},\mathbf{R}_{\mathrm{J'}})e^{i\mathbf{k}\cdot(\mathbf{R}_{\mathrm{J}}-\mathbf{R}_{\mathrm{J'}})}\hat{\psi}_n(\mathbf{x},\mathbf{k})\,\mathrm{d}\mathbf{x}\,, \\
&= -\sum_{J'}\int_{\Omega}\left(\frac{\partial}{\partial\mathbf{R}_{\mathrm{J'}}}\mathbf{S}^{\text{-T}}\right)_{\alpha}\left[\chi^{*}_{\mathrm{J'lm}}(\boldsymbol{\eta})(\mathbf{S}^{\mathrm{T}}\boldsymbol{\eta})_{\beta}e^{i\mathbf{k}\cdot(\mathbf{R}_{\mathrm{J}}-\mathbf{R}_{\mathrm{J'}})}\hat{\psi}_n(\boldsymbol{\eta}+\mathbf{R}_{\mathrm{J'}},\mathbf{k})\right]\mathrm{d}\boldsymbol{\eta} \\
&- \delta_{\alpha\beta}\int_{\Omega}\tilde{\chi}^{*}_{\mathrm{Jlm}}(\mathbf{x},\mathbf{R}_{\mathrm{J}},\mathbf{k})\hat{\psi}_n(\mathbf{x},\mathbf{k})\,\mathrm{d}\mathbf{x} \\
&= \sum_{J'}\int_{\Omega}\chi^{*}_{\mathrm{J'lm}}(\mathbf{x},\mathbf{R}_{\mathrm{J'}})\big(\mathbf{S}^{\mathrm{T}}\mathbf{R}_{\mathrm{J'}}-\mathbf{S}^{\mathrm{T}}\mathbf{x}\big)_{\beta}\,e^{i\mathbf{k}\cdot(\mathbf{R}_{\mathrm{J}}-\mathbf{R}_{\mathrm{J'}})}\boldsymbol{\nabla}_{\alpha}\hat{\psi}_n(\mathbf{x},\mathbf{k})\,\mathrm{d}\mathbf{x} \\
&- \delta_{\alpha\beta}\int_{\Omega}\tilde{\chi}^{*}_{\mathrm{Jlm}}(\mathbf{x},\mathbf{R}_{\mathrm{J}},\mathbf{k})\hat{\psi}_n(\mathbf{x},\mathbf{k})\,\mathrm{d}\mathbf{x}\,, \qquad (3.9)
\end{aligned}$$

where the second equality is obtained by again using the relation $\chi^{*}_{\mathrm{J'lm}}(\mathbf{x},\mathbf{R}_{\mathrm{J'}}) = \chi^{*}_{\mathrm{J'lm}}(\mathbf{S}^{\mathrm{T}}\mathbf{x} - \mathbf{S}^{\mathrm{T}}\mathbf{R}_{\mathrm{J'}})$, the third equality is obtained by using the chain-rule, the fourth equality is obtained by making the substitution $\mathbf{x} = \boldsymbol{\eta} + \mathbf{R}_{\mathrm{J'}}$, and the final equality is obtained by taking the derivative with respect to $\mathbf{R}_{\mathrm{J'}}$ and making the substitution $\boldsymbol{\eta} = \mathbf{x} - \mathbf{R}_{\mathrm{J'}}$.

The above reformulation is motivated by the fact that the original expression for $\chi^{\sigma}_{\alpha\beta}$ contains derivatives of the projectors, which are themselves highly localized and rapidly varying. Therefore, adopting the procedure previously used for the reformulation of the nonlocal component of the atomic forces [44, 45, 16], we have transferred the derivative on the nonlocal projectors (with respect to atomic position) to the orbitals (with respect to space). Since the orbitals are typically more smooth than the projectors, the accuracy of the stress tensor is significantly improved due to this reformulation, as demonstrated in Appendix B.

3.4 Stress tensor contribution $\sigma^{E_{el}}$

The contribution to the stress tensor arising from the total electrostatic energy:

$$
\begin{aligned}
\sigma^{E_{el}}_{\alpha\beta} &= \left.\frac{\partial E^F_{el}(\rho, \mathbf{R}^F, \phi)}{\partial \mathbf{F}_{\alpha\beta}}\right|_{\mathcal{G}} \\
&= \frac{\partial}{\partial \mathbf{F}_{\alpha\beta}}\Bigg(-\frac{1}{8\pi}\int_{\Omega^F} \left|\boldsymbol{\nabla}\phi(\mathbf{x}^F)\right|^2 \mathrm{d}\mathbf{x}^{\mathrm{F}} + \int_{\Omega^F} \big(\rho(\mathbf{x}^F) + b(\mathbf{x}^F, \mathbf{R}^F)\big)\phi(\mathbf{x}^F)\,\mathrm{d}\mathbf{x}^{\mathrm{F}} \\
&- E_{self}(\mathbf{R}^F) + E_c(\mathbf{R}^F)\Bigg)\Bigg|_{\mathcal{G}} \\
&= \frac{\partial}{\partial \mathbf{F}_{\alpha\beta}}\Bigg(-\frac{1}{8\pi}\int_{\Omega} \left|\mathbf{F}^{-\mathrm{T}}\boldsymbol{\nabla}\phi(\mathbf{Q}\mathbf{x})\right|^2 \det(\mathbf{F})\,\mathrm{d}\mathbf{x} + \int_{\Omega} \big(\rho(\mathbf{Q}\mathbf{x}) + b(\mathbf{Q}\mathbf{x}, \mathbf{Q}\mathbf{R})\big)\phi(\mathbf{Q}\mathbf{x})\det(\mathbf{F})\,\mathrm{d}\mathbf{x} \\
&- E_{self}(\mathbf{Q}\mathbf{R}) + E_c(\mathbf{Q}\mathbf{R})\Bigg)\Bigg|_{\mathcal{G}} \\
&= D_1 + D_2 + D_3 + D_4 + D_5 - \sigma^{E_{self}}_{\alpha\beta} + \sigma^{E_c}_{\alpha\beta}\,, \qquad (3.10)
\end{aligned}
$$

where

$$
\begin{aligned}
D_1 &= 2\sum_{n=1}^{N_s} \fint_{BZ}\int_{\Omega} \hat{\phi}(\mathbf{x}, \mathbf{R}) \left.\frac{\partial g_n(\mathbf{Q}^{-\mathrm{T}}\mathbf{k})}{\partial \mathbf{F}_{\alpha\beta}}\right|_{\mathcal{G}} \left|\hat{\psi}_n(\mathbf{x}, \mathbf{k})\right|^2 \mathrm{d}\mathbf{x}\,, \\
D_2 &= 2\sum_{n=1}^{N_s} \fint_{BZ}\int_{\Omega} \hat{\phi}(\mathbf{x}, \mathbf{R})\hat{g}_n(\mathbf{k}) \left.\frac{\partial \psi^*_n(\mathbf{Q}\mathbf{x}, \mathbf{Q}^{-\mathrm{T}}\mathbf{k})}{\partial \mathbf{F}_{\alpha\beta}}\right|_{\mathcal{G}} \hat{\psi}_n(\mathbf{x}, \mathbf{k})\,\mathrm{d}\mathbf{x}\,,
\end{aligned}
$$

$$
\begin{aligned}
D_3 &= 2\sum_{n=1}^{N_s} \fint_{BZ} \int_{\Omega} \hat{\phi}(\mathbf{x},\mathbf{R})\hat{\mathbf{g}}_n(\mathbf{k})\hat{\psi}_n^*(\mathbf{x},\mathbf{k}) \frac{\partial \psi_n(\mathbf{Q}\mathbf{x},\mathbf{Q}^{-\mathrm{T}}\mathbf{k})}{\partial \mathbf{F}_{\alpha\beta}}\bigg|_{\mathcal{G}} \mathrm{d}\mathbf{x}\,, \\
D_4 &= \int_{\Omega} \bigg(-\frac{1}{8\pi}\big|\boldsymbol{\nabla}\hat{\phi}(\mathbf{x},\mathbf{R})\big|^2 + \big(\hat{\rho}(\mathbf{x}) + b(\mathbf{x},\mathbf{R})\big)\hat{\phi}(\mathbf{x},\mathbf{R})\bigg) \frac{\partial\big(\det(\mathbf{F})\big)}{\partial \mathbf{F}_{\alpha\beta}}\bigg|_{\mathcal{G}} \mathrm{d}\mathbf{x} \\
&= \int_{\Omega} \frac{1}{2}\big(\hat{\rho}(\mathbf{x}) + b(\mathbf{x},\mathbf{R})\big)\hat{\phi}(\mathbf{x},\mathbf{R})\delta_{\alpha\beta}\,\mathrm{d}\mathbf{x}\,, \\
D_5 &= \int_{\Omega} \bigg(-\frac{1}{8\pi}\frac{\partial}{\partial \mathbf{F}_{\alpha\beta}}\Big[\boldsymbol{\nabla}^{\mathrm{T}}\mathbf{F}^{-1}\phi(\mathbf{Q}\mathbf{x})\mathbf{F}^{-\mathrm{T}}\boldsymbol{\nabla}\phi(\mathbf{Q}\mathbf{x})\Big]\bigg|_{\mathcal{G}} + \big(\hat{\rho}(\mathbf{x}) + b(\mathbf{x},\mathbf{R})\big)\frac{\partial \phi(\mathbf{Q}\mathbf{x})}{\partial \mathbf{F}_{\alpha\beta}}\bigg|_{\mathcal{G}} \\
&+ \frac{\partial b(\mathbf{Q}\mathbf{x},\mathbf{Q}\mathbf{R})}{\partial \mathbf{F}_{\alpha\beta}}\bigg|_{\mathcal{G}} \hat{\phi}(\mathbf{x},\mathbf{R})\bigg)\,\mathrm{d}\mathbf{x} \\
&= \int_{\Omega} \bigg(\frac{1}{4\pi}\boldsymbol{\nabla}_{\alpha}\hat{\phi}(\mathbf{x},\mathbf{R})\boldsymbol{\nabla}_{\beta}\hat{\phi}(\mathbf{x},\mathbf{R}) + \bigg(\frac{1}{4\pi}\nabla^2\hat{\phi}(\mathbf{x},\mathbf{R})\frac{\partial\phi(\mathbf{Q}\mathbf{x})}{\partial \mathbf{F}_{\alpha\beta}} + \big(\hat{\rho}(\mathbf{x}) + b(\mathbf{x},\mathbf{R})\big)\frac{\partial\phi(\mathbf{Q}\mathbf{x})}{\partial \mathbf{F}_{\alpha\beta}}\bigg)\bigg|_{\mathcal{G}} \\
&+ \sum_I \boldsymbol{\nabla}_{\alpha} b_I(\mathbf{x},\mathbf{R}_I)\big(\mathbf{S}^{\mathrm{T}}\mathbf{x} - \mathbf{S}^{\mathrm{T}}\mathbf{R}_I\big)_{\beta}\hat{\phi}(\mathbf{x},\mathbf{R})\bigg)\,\mathrm{d}\mathbf{x} \\
&= \int_{\Omega} \bigg(\frac{1}{4\pi}\boldsymbol{\nabla}_{\alpha}\hat{\phi}(\mathbf{x},\mathbf{R})\boldsymbol{\nabla}_{\beta}\hat{\phi}(\mathbf{x},\mathbf{R}) + \sum_I \boldsymbol{\nabla}_{\alpha} b_I(\mathbf{x},\mathbf{R}_I)\big(\mathbf{S}^{\mathrm{T}}\mathbf{x} - \mathbf{S}^{\mathrm{T}}\mathbf{R}_I\big)_{\beta}\hat{\phi}(\mathbf{x},\mathbf{R})\bigg)\,\mathrm{d}\mathbf{x}\,, \\
\sigma_{\alpha\beta}^{E_{self}} &= \frac{\partial}{\partial \mathbf{F}_{\alpha\beta}}\bigg(\frac{1}{2}\sum_I \int_{\Omega} b_I(\mathbf{Q}\mathbf{x},\mathbf{Q}\mathbf{R}_I)V_I(\mathbf{Q}\mathbf{x},\mathbf{Q}\mathbf{R}_I)\det(\mathbf{F})\,\mathrm{d}\mathbf{x}\bigg)\bigg|_{\mathrm{G}} \\
&= \frac{1}{2}\sum_I \int_{\Omega} \bigg(\boldsymbol{\nabla}_{\alpha} b_I(\mathbf{x},\mathbf{R}_I)\big(\mathbf{S}^{\mathrm{T}}\mathbf{x} - \mathbf{S}^{\mathrm{T}}\mathbf{R}_I\big)_{\beta} V_I(\mathbf{x},\mathbf{R}_I) + b_I(\mathbf{x},\mathbf{R}_I)\boldsymbol{\nabla}_{\alpha}V_I(\mathbf{x},\mathbf{R}_I) \\
&\times \big(\mathbf{S}^{\mathrm{T}}\mathbf{x} - \mathbf{S}^{\mathrm{T}}\mathbf{R}_I\big)_{\beta}\bigg)\,\mathrm{d}\mathbf{x} + \delta_{\alpha\beta}E_{self}(\mathbf{R})\,.
\end{aligned}
$$

The expression for $\sigma_{\alpha\beta}^{E_c}$ can be found in Appendix A. In obtaining the terms D_1, D_2, and D_3, we have used the relation in Equation 3.6. It is important to note that using Gauss' divergence theorem and the chain rule, it is possible to show that $\sigma_{\alpha\beta}^{E_{self}} = 0$, consistent with the result obtained in the context of the planewave method [46]. However, due to the inexact nature of the chain rule within the finite-difference approximation, $\sigma_{\alpha\beta}^{E_{self}}$ can take significant values, as shown in Appendix C. Therefore, we utilize the above formulation for $\sigma_{\alpha\beta}^{E_{self}}$, which we have found to be particularly well suited to error cancellation with the other terms.

3.5 Stress tensor contribution σ^S

The contribution to the stress tensor arising from the electronic entropy energy:

$$\begin{aligned}
\sigma^S_{\alpha\beta} &= \left.\frac{\partial S^F(\mathbf{g})}{\partial \mathbf{F}_{\alpha\beta}}\right|_{\mathcal{G}} \\
&= \left.\frac{\partial}{\partial \mathbf{F}_{\alpha\beta}}\left(-\,2\sigma \sum_{n=1}^{N_s} \fint_{BZ^F} \Big(g_n(\mathbf{k}^F)\log g_n(\mathbf{k}^F) + \big(1-g_n(\mathbf{k}^F)\big)\log\big(1-g_n(\mathbf{k}^F)\big)\Big)\,\mathrm{d}\mathbf{k}^{\mathrm{F}}\right)\right|_{\mathcal{G}} \\
&= \left.\frac{\partial}{\partial \mathbf{F}_{\alpha\beta}}\left(-\,2\sigma \sum_{n=1}^{N_s} \fint_{BZ} \Big(g_n(\mathbf{Q}^{-\mathrm{T}}\mathbf{k})\log g_n(\mathbf{Q}^{-\mathrm{T}}\mathbf{k}) + \big(1-g_n(\mathbf{Q}^{-\mathrm{T}}\mathbf{k})\big)\right.\right. \\
&\times \left.\left.\log\big(1-g_n(\mathbf{Q}^{-\mathrm{T}}\mathbf{k})\big)\Big)\,\mathrm{d}\mathbf{k}\right)\right|_{\mathcal{G}} \\
&= -2\sigma \sum_{n=1}^{N_s} \fint_{BZ} \left.\frac{\partial g_n(\mathbf{Q}^{-\mathrm{T}}\mathbf{k})}{\partial \mathbf{F}_{\alpha\beta}}\right|_{\mathcal{G}} \log\left(\frac{\hat{g}_n(\mathbf{k})}{1-\hat{g}_n(\mathbf{k})}\right)\mathrm{d}\mathbf{k}\,. \qquad (3.11)
\end{aligned}$$

3.6 Stress tensor contribution $\sigma^{\lambda_{mn}}$

The contribution to the stress tensor arising from the constraint on the orthonormality of the orbitals:

$$\begin{aligned}
\sigma^{\lambda_{mn}}_{\alpha\beta} &= \left.\frac{\partial}{\partial \mathbf{F}_{\alpha\beta}}\left(2\sum_{mn} \fint_{BZ^F} \lambda_{mn}(\mathbf{k}^F)\left(\int_{\Omega^F} \psi^*_m(\mathbf{x}^F,\mathbf{k}^F)\psi_n(\mathbf{x}^F,\mathbf{k}^F)\,\mathrm{d}\mathbf{x}^{\mathrm{F}} - \delta_{mn}\right)\mathrm{d}\mathbf{k}^{\mathrm{F}}\right)\right|_{\mathcal{G}} \\
&= \left.\frac{\partial}{\partial \mathbf{F}_{\alpha\beta}}\left(2\sum_{mn} \fint_{BZ} \lambda_{mn}(\mathbf{Q}^{-\mathrm{T}}\mathbf{k})\left(\int_{\Omega} \psi^*_m(\mathbf{Q}\mathbf{x},\mathbf{Q}^{-\mathrm{T}}\mathbf{k})\psi_n(\mathbf{Q}\mathbf{x},\mathbf{Q}^{-\mathrm{T}}\mathbf{k})\det(\mathbf{F})\,\mathrm{d}\mathbf{x}\right.\right.\right. \\
&- \left.\left.\left.\delta_{mn}\right)\mathrm{d}\mathbf{k}\right)\right|_{\mathcal{G}} \\
&= F_1 + F_2 + F_3 + F_4\,, \qquad (3.12)
\end{aligned}$$

where

$$\begin{aligned}
F_1 &= 2\sum_{mn} \fint_{BZ} \left.\frac{\partial \lambda_{mn}(\mathbf{Q}^{-\mathrm{T}}\mathbf{k})}{\partial \mathbf{F}_{\alpha\beta}}\right|_{\mathcal{G}} \left(\int_{\Omega} \hat{\psi}^*_m(\mathbf{x},\mathbf{k})\hat{\psi}_n(\mathbf{x},\mathbf{k})\,\mathrm{d}\mathbf{x} - \delta_{mn}\right)\mathrm{d}\mathbf{k} \\
&= 0\,,
\end{aligned}$$

$$
\begin{aligned}
F_2 &= 2\sum_m \fint_{BZ} \hat{\lambda}_m(\mathbf{k}) \int_\Omega \frac{\partial \psi_m^*(\mathbf{Q}\mathbf{x}, \mathbf{Q}^{-\mathrm{T}}\mathbf{k})}{\partial \mathbf{F}_{\alpha\beta}}\bigg|_{\mathcal{G}} \hat{\psi}_m(\mathbf{x},\mathbf{k})\,\mathrm{d}\mathbf{x}\,\mathrm{d}\mathbf{k}\,,\\
F_3 &= 2\sum_n \fint_{BZ} \hat{\lambda}_n(\mathbf{k}) \int_\Omega \hat{\psi}_n^*(\mathbf{x},\mathbf{k}) \frac{\partial \psi_n(\mathbf{Q}\mathbf{x}, \mathbf{Q}^{-\mathrm{T}}\mathbf{k})}{\partial \mathbf{F}_{\alpha\beta}}\bigg|_{\mathcal{G}} \mathrm{d}\mathbf{x}\,\mathrm{d}\mathbf{k}\,,\\
F_4 &= 2\sum_m \fint_{BZ} \hat{\lambda}_m(\mathbf{k}) \int_\Omega \hat{\psi}_m^*(\mathbf{x},\mathbf{k})\hat{\psi}_m(\mathbf{x},\mathbf{k}) \frac{\partial\big(\det(\mathbf{F})\big)}{\partial \mathbf{F}_{\alpha\beta}}\bigg|_{\mathcal{G}} \mathrm{d}\mathbf{x}\,\mathrm{d}\mathbf{k}\,,\\
&= 2\sum_m \fint_{BZ} \hat{\lambda}_m(\mathbf{k}) \int_\Omega \hat{\psi}_m^*(\mathbf{x},\mathbf{k})\hat{\psi}_m(\mathbf{x},\mathbf{k})\delta_{\alpha\beta}\,\mathrm{d}\mathbf{x}\,\mathrm{d}\mathbf{k}\,.
\end{aligned}
$$

3.7 Stress tensor contribution σ^{λ_f}

The contribution to the stress tensor arising from the constraint on the total number of electrons:

$$
\begin{aligned}
\sigma_{\alpha\beta}^{\lambda_f} &= \frac{\partial}{\partial \mathbf{F}_{\alpha\beta}}\left(\lambda_f\left(2\sum_{n=1}^{N_s}\fint_{BZ^F} g_n(\mathbf{k}^F)\,\mathrm{d}\mathbf{k} - N_e\right)\right)\bigg|_{\mathcal{G}}\\
&= \frac{\partial}{\partial \mathbf{F}_{\alpha\beta}}\left(\lambda_f\left(2\sum_{n=1}^{N_s}\fint_{BZ} g_n(\mathbf{Q}^{-\mathrm{T}}\mathbf{k})\,\mathrm{d}\mathbf{k} - N_e\right)\right)\bigg|_{\mathcal{G}}\\
&= 2\,\hat{\lambda}_f \sum_{n=1}^{N_s}\fint_{BZ} \frac{\partial g_n(\mathbf{Q}^{-\mathrm{T}}\mathbf{k})}{\partial \mathbf{F}_{\alpha\beta}}\bigg|_{\mathcal{G}} \mathrm{d}\mathbf{k}\,. \qquad (3.13)
\end{aligned}
$$

3.8 Total stress tensor

It follows from Equation 3.1 and Equation 3.2 that the total stress can be written in terms of the various contributions derived in the previous sections as

$$
\begin{aligned}
\boldsymbol{\sigma}_{\alpha\beta} &= \frac{1}{|\Omega|}\left[\sigma_{\alpha\beta}^{T_s} + \sigma_{\alpha\beta}^{E_{xc}} + \sigma_{\alpha\beta}^{E_{nl}} + \sigma_{\alpha\beta}^{E_{el}} - \sigma_{\alpha\beta}^{S} - \sigma_{\alpha\beta}^{\lambda_{mn}} - \sigma_{\alpha\beta}^{\lambda_f}\right]\\
&= \frac{1}{|\Omega|}\left[\sum_{i=1}^{5}(A_i + B_i + C_i + D_i) - \sigma_{\alpha\beta}^{E_{self}} + \sigma_{\alpha\beta}^{E_c} - \sigma_{\alpha\beta}^{S} - \sum_{i=1}^{4} F_i - \sigma_{\alpha\beta}^{\lambda_f}\right] \qquad (3.14)
\end{aligned}
$$

As a consequence of the Euler-Lagrange equations in Equation 2.9–Equation 2.11, we have the relations:

$$
\begin{aligned}
A_1 + B_1 + C_1 + D_1 - \sigma^{S}_{\alpha\beta} - \sigma^{\lambda_f}_{\alpha\beta} &= 0\,, && (3.15)\\
A_2 + B_2 + C_2 + D_2 - F_2 &= 0 && (3.16)\\
A_3 + B_3 + C_3 + D_3 - F_3 &= 0\,, && (3.17)\\
A_4 + B_4 + C_4 + D_4 - F_4 &= \delta_{\alpha\beta}\Bigg[E_{xc}(\hat{\rho}, \boldsymbol{\nabla}\hat{\rho}) - \int_\Omega V_{xc}\big(\hat{\rho}(\mathbf{x}), \boldsymbol{\nabla}\hat{\rho}(\mathbf{x})\big)\hat{\rho}(\mathbf{x})\,\mathrm{d}\mathbf{x}\\
&\quad + E_{nl}(\hat{\boldsymbol{\Psi}}, \hat{\mathbf{g}}, \mathbf{R})\\
&\quad + \frac{1}{2}\int_\Omega \big(b(\mathbf{x},\mathbf{R}) - \hat{\rho}(\mathbf{x})\big)\hat{\phi}(\mathbf{x},\mathbf{R})\,\mathrm{d}\mathbf{x}\Bigg]\,. && (3.18)
\end{aligned}
$$

Inserting the above relations and those from Equation 3.4, Equation 3.5, Equation 3.7, Equation 3.10, Equation 3.11, Equation 3.12, and Equation 3.13 into Equation 3.14, we arrive at the expression for the total stress:

$$
\begin{aligned}
\sigma_{\alpha\beta} &= \frac{1}{|\Omega|}\Bigg[-2\sum_{n=1}^{N_s} \fint_{BZ} \hat{\mathbf{g}}_n(\mathbf{k}) \int_\Omega \boldsymbol{\nabla}_\alpha \hat{\psi}^*_n(\mathbf{x},\mathbf{k})\boldsymbol{\nabla}_\beta\hat{\psi}_n(\mathbf{x},\mathbf{k})\,\mathrm{d}\mathbf{x}\,\mathrm{d}\mathbf{k} + \delta_{\alpha\beta}\Bigg(E_{xc}(\hat{\rho},\boldsymbol{\nabla}\hat{\rho})\\
&- \int_\Omega V_{xc}\big(\hat{\rho}(\mathbf{x}),\boldsymbol{\nabla}\hat{\rho}(\mathbf{x})\big)\hat{\rho}(\mathbf{x})\,\mathrm{d}\mathbf{x}\Bigg) - \int_\Omega \hat{\rho}(\mathbf{x})\frac{\partial\varepsilon_{xc}\big(\hat{\rho}(\mathbf{x}),\boldsymbol{\nabla}\hat{\rho}(\mathbf{x})\big)}{\partial\big(\boldsymbol{\nabla}_\beta\hat{\rho}(\mathbf{x})\big)}\boldsymbol{\nabla}_\alpha\hat{\rho}(\mathbf{x})\,\mathrm{d}\mathbf{x} - \delta_{\alpha\beta}E_{nl}(\hat{\boldsymbol{\Psi}},\hat{\mathbf{g}},\mathbf{R})\\
&- 4\sum_{n=1}^{N_s}\fint_{BZ}\hat{\mathbf{g}}_n(\mathbf{k})\sum_J\sum_{lm}\gamma_{\mathrm{Jl}}\Re\Bigg[\sum_{J'}\int_\Omega \chi^*_{\mathrm{J'lm}}(\mathbf{x},\mathbf{R}_{\mathrm{J'}})e^{i\mathbf{k}\cdot(\mathbf{R}_{\mathrm{J}}-\mathbf{R}_{\mathrm{J'}})}\big(\mathbf{S}^{\mathrm{T}}\mathbf{x} - \mathbf{S}^{\mathrm{T}}\mathbf{R}_{\mathrm{J'}}\big)_\beta\\
&\times \boldsymbol{\nabla}_\alpha\hat{\psi}_n(\mathbf{x},\mathbf{k})\,\mathrm{d}\mathbf{x}\Bigg(\int_\Omega \tilde{\chi}_{\mathrm{Jlm}}(\mathbf{x},\mathbf{R}_{\mathrm{J}},\mathbf{k})\hat{\psi}^*_n(\mathbf{x},\mathbf{k})\,\mathrm{d}\mathbf{x}\Bigg)\Bigg]\,\mathrm{d}\mathbf{k} + \frac{1}{4\pi}\int_\Omega \boldsymbol{\nabla}_\alpha\hat{\phi}(\mathbf{x},\mathbf{R})\boldsymbol{\nabla}_\beta\hat{\phi}(\mathbf{x},\mathbf{R})\,\mathrm{d}\mathbf{x}\\
&+ \sum_I\int_\Omega \boldsymbol{\nabla}_\alpha b_I(\mathbf{x},\mathbf{R}_I)\big(\mathbf{S}^{\mathrm{T}}\mathbf{x} - \mathbf{S}^{\mathrm{T}}\mathbf{R}_I\big)_\beta\Big(\hat{\phi}(\mathbf{x},\mathbf{R}) - \frac{1}{2}V_I(\mathbf{x},\mathbf{R}_I)\Big)\,\mathrm{d}\mathbf{x}\\
&- \frac{1}{2}\sum_I\int_\Omega \boldsymbol{\nabla}_\alpha V_I(\mathbf{x},\mathbf{R}_I)\big(\mathbf{S}^{\mathrm{T}}\mathbf{x} - \mathbf{S}^{\mathrm{T}}\mathbf{R}_I\big)_\beta b_I(\mathbf{x},\mathbf{R}_I)\,\mathrm{d}\mathbf{x} + \frac{1}{2}\delta_{\alpha\beta}\int_\Omega \big(b(\mathbf{x},\mathbf{R}) - \hat{\rho}(\mathbf{x})\big)\hat{\phi}(\mathbf{x},\mathbf{R})\,\mathrm{d}\mathbf{x}\\
&- \delta_{\alpha\beta}E_{self}(\mathbf{R}) + \sigma^{E_c}_{\alpha\beta}\Bigg]\,. \qquad (3.19)
\end{aligned}
$$

The resulting expression for the pressure:

$$
\begin{aligned}
P &= -\frac{1}{3}\sum_{i=1}^{3}\sigma_{ii} \\
&= -\frac{1}{3|\Omega|}\Bigg[-4\sum_{n=1}^{N_s}\fint_{BZ}\hat{\mathbf{g}}_n(\mathbf{k})\hat{\lambda}_n(\mathbf{k})\,\mathrm{d}\mathbf{k} + 3E_{xc}(\hat{\rho},\boldsymbol{\nabla}\hat{\rho}) - \int_\Omega\Big(V_{xc}\big(\hat{\rho}(\mathbf{x}),\boldsymbol{\nabla}\hat{\rho}(\mathbf{x})\big) \\
&+ \frac{\partial\varepsilon_{xc}\big(\hat{\rho}(\mathbf{x}),\boldsymbol{\nabla}\hat{\rho}(\mathbf{x})\big)}{\partial\big(\boldsymbol{\nabla}\hat{\rho}(\mathbf{x})\big)}\cdot\boldsymbol{\nabla}\hat{\rho}(\mathbf{x})\Big)\hat{\rho}(\mathbf{x})\,\mathrm{d}\mathbf{x} - E_{nl}(\hat{\boldsymbol{\Psi}},\hat{\mathbf{g}},\mathbf{R}) - 4\sum_{n=1}^{N_s}\fint_{BZ}\hat{\mathbf{g}}_n(\mathbf{k})\sum_{J}\sum_{lm}\gamma_{\mathrm{Jl}} \\
&\times \Re\Bigg[\Bigg(\sum_{J'}\int_\Omega\chi^*_{\mathrm{J'lm}}(\mathbf{x},\mathbf{R}_{\mathrm{J'}})e^{i\mathbf{k}\cdot(\mathbf{R}_{\mathrm{J}}-\mathbf{R}_{\mathrm{J'}})}\mathbf{S}^{\mathrm{T}}\big(\mathbf{x}-\mathbf{R}_{\mathrm{J'}}\big)\cdot\boldsymbol{\nabla}\hat{\psi}_n(\mathbf{x},\mathbf{k})\,\mathrm{d}\mathbf{x}\Bigg)\Bigg(\int_\Omega\tilde{\chi}_{\mathrm{Jlm}}(\mathbf{x},\mathbf{R}_{\mathrm{J}},\mathbf{k}) \\
&\times \hat{\psi}^*_n(\mathbf{x},\mathbf{k})\,\mathrm{d}\mathbf{x}\Bigg)\Bigg]\,\mathrm{d}\mathbf{k} + \frac{1}{4\pi}\int_\Omega\big|\boldsymbol{\nabla}\hat{\phi}(\mathbf{x},\mathbf{R})\big|^2\,\mathrm{d}\mathbf{x} + \sum_I\int_\Omega\boldsymbol{\nabla}b_I(\mathbf{x},\mathbf{R}_I)\cdot\big(\mathbf{S}^{\mathrm{T}}\mathbf{x}-\mathbf{S}^{\mathrm{T}}\mathbf{R}_I\big) \\
&\times \Big(\hat{\phi}(\mathbf{x},\mathbf{R}) - \frac{1}{2}V_I(\mathbf{x},\mathbf{R}_I)\Big)\,\mathrm{d}\mathbf{x} - \frac{1}{2}\sum_I\int_\Omega\boldsymbol{\nabla}V_I(\mathbf{x},\mathbf{R}_I)\cdot\big(\mathbf{S}^{\mathrm{T}}\mathbf{x}-\mathbf{S}^{\mathrm{T}}\mathbf{R}_I\big)b_I(\mathbf{x},\mathbf{R}_I)\,\mathrm{d}\mathbf{x} \\
&+ \frac{1}{2}\int_\Omega\big(\hat{\rho}(\mathbf{x})+3b(\mathbf{x},\mathbf{R})\big)\hat{\phi}(\mathbf{x},\mathbf{R})\,\mathrm{d}\mathbf{x} - 3E_{self}(\mathbf{R}) + \sum_{i=1}^{3}\sigma_{ii}^{E_c}\Bigg]. \qquad (3.20)
\end{aligned}
$$

The above expressions for the stress and pressure can be evaluated in $\mathcal{O}(N)$ operations and are applicable for the general case of a non-orthogonal crystal system with Brillouin zone sampling and for the choice of a semilocal exchange-correlation functional. Indeed, the expression for a Γ-point calculation can be obtained by dropping the volume-average integral over the Brillouin zone and setting $\mathbf{k} = \mathbf{0}$ in the expressions. In addition, the expression for the choice of a local exchange-correlation functional such as the local density approximation (LDA) [2] can be obtained by dropping $\boldsymbol{\nabla}\hat{\rho}$ and the associated derivative terms.

CHAPTER 4

RESULTS AND DISCUSSION

In this section, we verify the accuracy and efficiency of the proposed formulation for calculating the stress tensor in real-space DFT calculations. For this purpose, we develop an implementation in the M-SPARC [47] prototype code, a serial implementation of the large-scale real-space DFT code SPARC [15, 16, 17]. The Poisson problem in Equation 2.11 is solved using the Alternating Anderson-Richardson (AAR) method [48, 49]. The electronic ground-state is calculated using the Chebyshev-filtered subspace iteration (CheFSI) [50, 51], with acceleration provided by the restarted Periodic Pulay method [52, 53]. In all simulations, we employ a twelfth-order accurate finite-difference discretization, norm-conserving Troullier-Martins pseudopotentials [54], trapezoidal rule for all integrations in real space, and the Monkhorst-Pack [55] grid for integration over the Brillouin zone. A more detailed description of the underlying finite-difference formulation and implementation can be found in our previous work [15, 16].

As representative examples, we consider the following systems: (i) hexagonal close packed (hcp) titanium with equilibrium lattice parameters: $L_1 = 5.47$ Bohr, $L_2 = 5.47$ Bohr, $L_3 = 8.85$ Bohr, $\theta_1 = \theta_2 = 90^\circ$, and $\theta_3 = 120^\circ$; (ii) diamond cubic (dc) germanium with equilibrium lattice parameters: $L_1 = L_2 = L_3 = 10.74$ Bohr, and $\theta_1 = \theta_2 = \theta_3 = 90^\circ$; and (iii) triclinic titanium with equilibrium lattice parameters: $L_1 = 5.47$ Bohr, $L_2 = 5.47$ Bohr, $L_3 = 8.85$ Bohr, $\theta_1 = 97^\circ$, $\theta_2 = 82^\circ$, and $\theta_3 = 107^\circ$. We employ the PW [56] variant of LDA and the PBE [57] variant of GGA as exchange-correlation functionals for the titanium and germanium systems, respectively. Wherever suitable, we compare with the planewave code ABINIT [58], wherein we use planewave cutoffs of 70 Ha and 30 Ha for the titanium and germanium systems, respectively, which results in the stresses being converged to within 0.01 %.

4.1 Convergence of stress tensor with discretization

First, we verify convergence of the stress tensor with respect to spatial discretization. For this study, we choose a 2-atom unit cell of hcp titanium uniformly expanded by 1%, a 2-atom unit cell of triclinic titanium, and an 8-atom unit cell of dc germanium uniformly compressed by 1%. We employ $6 \times 6 \times 6$ and $5 \times 5 \times 5$ **k**-point grids for the titanium and germanium systems, respectively. In Figure 4.1, we present the error in the calculated stress tensor as a function of mesh size. The error is defined with respect to reference M-SPARC results that are converged to 0.001% accuracy, which in turn agree with highly converged ABINIT results to within 0.2%. It is clear that there is systematic convergence of the computed stress tensor. On performing a linear fit to the data, we obtain convergence rates of approximately $\mathcal{O}(h^{10})$ with respect to mesh size. These results demonstrate that high rates of convergence—similar to those obtained for the energy and atomic forces [16, 18]—can be obtained for the stress tensor within the proposed formulation.

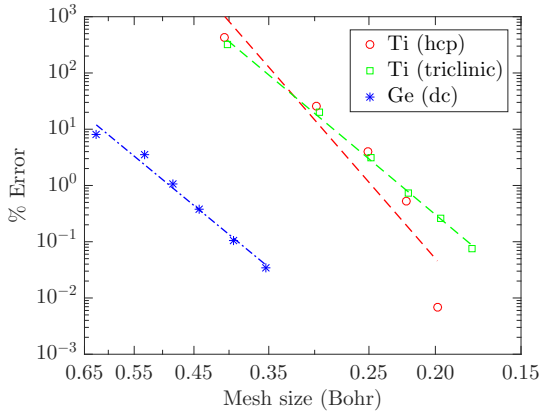

Figure 4.1: Convergence of the stress tensor with mesh size for the hcp titanium, triclinic titanium, and dc germanium systems. The error is defined to be magnitude of the maximum difference in any component. The straight lines represent linear fits to the data.

4.2 Cell optimization using the stress tensor

Next, we verify the accuracy of the computed stress tensor for performing cell optimization. For this study, we consider a 2-atom unit cell of hcp titanium and an 8-atom unit cell of

dc germanium, with $6 \times 6 \times 6$ and $5 \times 5 \times 5$ $\mathbf{k}$-point grids for Brillouin zone integration, respectively. In Figure 4.2, we plot the variation in energy and pressure as a function of the unit cell volume as computed by M-SPARC and ABINIT. Specifically, we plot the computed energy and its cubic spline fit in Figure 4.2a, and the computed pressure and the derivative of the cubic spline fit to the energy in Figure 4.2b. Note that we have employed a constant number of grid points in M-SPARC, i.e., they are independent of the unit cell volume and correspond to mesh sizes of 0.22 and 0.44 Bohr for the titanium and germanium systems at their equilibrium volumes, respectively. It is clear from the results that there is excellent agreement between ABINIT and M-SPARC, with the results being practically indistinguishable. In particular, as determined from the data in Figure 4.2b, the difference in equilibrium lattice constants predicted by M-SPARC and ABINIT for the titanium and germanium systems are 0.0003 Bohr and 0.003 Bohr, respectively, and the corresponding difference in the bulk modulus is 0.004 GPa and 0.3 GPa, respectively. The Pulay stress [59] at the chosen mesh sizes is estimated to be 0.014 GPa and 0.0086 GPa for the titanium and germanium systems, respectively.[1]

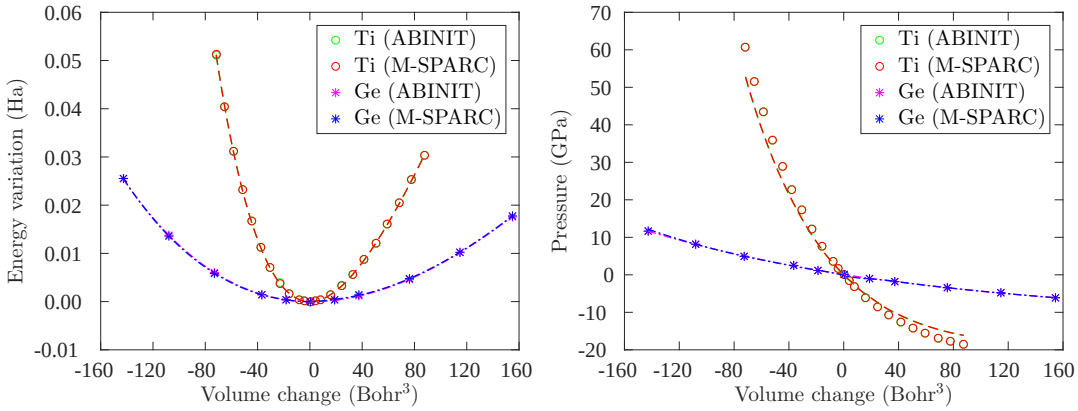

(a) Computed energy difference and its cubic spline fit

(b) Computed pressure and the derivative of the cubic spline fit to the energy

Figure 4.2: Variation in the energy difference and pressure computed by ABINIT and M-SPARC as a function of volume change for the hcp titanium and dc germanium systems. The volume change and energy difference are defined with respect to the equilibrium system, i.e., cell corresponding to zero stress.

[1]The Pulay stress is estimated using the technique described in the VASP [3] manual.

It is also clear from the results in Figure 4.2 that the computed energy and pressure are consistent within the proposed formulation. This is also true for the complete stress tensor, as verified by the results in Table 4.1 for the 2-atom triclinic titanium system with $6 \times 6 \times 6$ $\mathbf{k}$-point sampling. In particular, the maximum difference between the computed stress tensor and that obtained from the numerical derivative of the energy is less than 1%.

Table 4.1: Computed stress tensor and that obtained from the numerical derivative of the energy for the triclinic titanium system by M-SPARC. All stress component values are reported in GPa.

	σ_{11}	σ_{12}	σ_{13}	σ_{22}	σ_{23}	σ_{33}
Computed	6.884	4.371	-3.237	9.610	2.476	5.104
Numerical derivative	6.852	4.351	-3.260	9.551	2.493	5.053

4.3 Stress tensor in ab-initio molecular dynamics

Finally, we verify the ability of the proposed formulation to accurately calculate the stress tensor in AIMD simulations. To do so, we consider 128-atom hcp titanium and 216-atom dc germanium systems with the atoms randomly perturbed by up to 10% of nearest neighbor distance and perform Γ-point calculations, as is typical in AIMD simulations. In M-SPARC, we employ mesh sizes of $h = 0.21$ Bohr and $h = 0.44$ Bohr for the titanium and germanium systems, respectively. It is clear from the results presented in Table 4.2 that there is very good agreement between M-SPARC and ABINIT, with the maximum difference in any stress component being 0.9 %, an accuracy representative of those desired in practical calculations. Note that as the mesh is refined in M-SPARC, the agreement with ABINIT further increases. Also note that the calculation of the stress tensor takes less than 1% of the total simulation time in M-SPARC, which verifies the efficiency of the proposed formulation for real-space DFT calculations.

Table 4.2: Stress tensor computed by M-SPARC and ABINIT for the hcp titanium and dc germanium systems. All stress component values are reported in GPa.

		σ_{11}	σ_{12}	σ_{13}	σ_{22}	σ_{23}	σ_{33}
Ti_{128}	M-SPARC	-6.175	0.585	0.235	-5.219	0.000	-5.981
	ABINIT	-6.159	0.580	0.235	-5.251	0.000	-6.038
Ge_{216}	M-SPARC	-23.569	1.933	2.551	-27.397	-3.746	-25.032
	ABINIT	-23.569	1.933	2.551	-27.398	-3.746	-25.034

CHAPTER 5
CONCLUSION

In this thesis, an accurate and efficient formulation of the stress tensor for Kohn-Sham DFT calculations employing the real-space finite-difference method is presented. Specifically, while employing a local formulation of the electrostatics, a linear-scaling expression for the stress tensor that is applicable to simulations with unit cells of arbitrary symmetry, semilocal exchange-correlation functionals, and Brillouin zone integration is derived. In particular, the contributions to the stress tensor arising from the self energy and the nonlocal pseudopotential energy are rewritten so as to make them compliant with the real-space method, thereby achieving up to three orders of magnitude improvement in the accuracy of the computed stresses. Through selected examples representative of static DFT calculations, the accuracy and efficiency of the expression derived for the stress tensor is verified. In particular, it is demonstrated that the proposed formulation obtains high rates of convergence with spatial discretization and that there is consistency between the computed energy and stress tensor, while maintaining very good agreement with reference planewave results. Overall, this work overcomes one of the limitations of real-space approaches, i.e., inability to compute the stress tensor, making them an even more attractive choice for DFT calculations.

Appendices

APPENDIX A

STRESS TENSOR CONTRIBUTION σ^{E_C}

The repulsive energy correction for overlapping pseudocharges takes the form [42, 43]:

$$\begin{aligned} E_c(\mathbf{R}) &= \frac{1}{2}\int_\Omega \big(\tilde{b}(\mathbf{x},\mathbf{R}) + b(\mathbf{x},\mathbf{R})\big)V_c(\mathbf{x},\mathbf{R})\,\mathrm{d}\mathbf{x} + \frac{1}{2}\sum_I \int_\Omega b_I(\mathbf{x},\mathbf{R}_I)V_I(\mathbf{x},\mathbf{R}_I)\,\mathrm{d}\mathbf{x} \\ &- \frac{1}{2}\sum_I \int_\Omega \tilde{b}_I(\mathbf{x},\mathbf{R}_I)\tilde{V}_I(\mathbf{x},\mathbf{R}_I)\,\mathrm{d}\mathbf{x}\,, \end{aligned} \tag{A.1}$$

where $V_c(\mathbf{x},\mathbf{R}) = \sum_I \big(\tilde{V}_I(\mathbf{x},\mathbf{R}_I) - V_I(\mathbf{x},\mathbf{R}_I)\big)$; $\tilde{b} = \sum_I \tilde{b}_I$ denotes the total reference pseudocharge density of the nuclei with $\tilde{b}_I$ being the reference pseudocharge density of the I^{th} nucleus that generates the potential $\tilde{V}_I$; and the summation index I runs over all atoms in $\mathbb{R}^3$. The contribution to the stress tensor arising from this repulsive energy correction:

$$\begin{aligned} \sigma^{E_c}_{\alpha\beta} &= \left.\frac{\partial E_c(\mathbf{R}^F)}{\partial \mathbf{F}_{\alpha\beta}}\right|_{\mathcal{G}} \\ &= \frac{\partial}{\partial \mathbf{F}_{\alpha\beta}}\Bigg(\frac{1}{2}\int_{\Omega^F}\big(\tilde{b}(\mathbf{x}^F,\mathbf{R}^F) + b(\mathbf{x}^F,\mathbf{R}^F)\big)V_c(\mathbf{x}^F,\mathbf{R}^F)\,\mathrm{d}\mathbf{x}^{\mathrm{F}} \\ &+ \frac{1}{2}\sum_I \int_{\Omega^F} b_I(\mathbf{x}^F,\mathbf{R}^F_I)V_I(\mathbf{x}^F,\mathbf{R}^F_I)\,\mathrm{d}\mathbf{x}^{\mathrm{F}} - \frac{1}{2}\sum_I\int_{\Omega^F}\tilde{b}_I(\mathbf{x}^F,\mathbf{R}^F_I)\tilde{V}_I(\mathbf{x}^F,\mathbf{R}^F_I)\,\mathrm{d}\mathbf{x}^{\mathrm{F}}\Bigg)\Bigg|_{\mathcal{G}} \\ &= \frac{\partial}{\partial \mathbf{F}_{\alpha\beta}}\Bigg(\frac{1}{2}\int_\Omega\big(\tilde{b}(\mathbf{Q}\mathbf{x},\mathbf{Q}\mathbf{R}) + b(\mathbf{Q}\mathbf{x},\mathbf{Q}\mathbf{R})\big)V_c(\mathbf{Q}\mathbf{x},\mathbf{Q}\mathbf{R})\det(\mathbf{F})\,\mathrm{d}\mathbf{x} + \frac{1}{2}\sum_I\int_\Omega b_I(\mathbf{Q}\mathbf{x},\mathbf{Q}\mathbf{R}_I) \\ &\times V_I(\mathbf{Q}\mathbf{x},\mathbf{Q}\mathbf{R}_I)\det(\mathbf{F})\,\mathrm{d}\mathbf{x} - \frac{1}{2}\sum_I\int_\Omega\tilde{b}_I(\mathbf{Q}\mathbf{x},\mathbf{Q}\mathbf{R}_I)\tilde{V}_I(\mathbf{Q}\mathbf{x},\mathbf{Q}\mathbf{R}_I)\det(\mathbf{F})\,\mathrm{d}\mathbf{x}\Bigg)\Bigg|_{\mathcal{G}} \\ &= \frac{1}{2}\sum_I\int_\Omega\Big(\boldsymbol{\nabla}_\alpha\tilde{b}_I(\mathbf{x},\mathbf{R}_I)\big(V_c(\mathbf{x},\mathbf{R}) - \tilde{V}_I(\mathbf{x},\mathbf{R}_I)\big) + \boldsymbol{\nabla}_\alpha b_I(\mathbf{x},\mathbf{R}_I)\big(V_c(\mathbf{x},\mathbf{R}) + V_I(\mathbf{x},\mathbf{R}_I)\big) \\ &+ \big(b(\mathbf{x},\mathbf{R}) + \tilde{b}(\mathbf{x},\mathbf{R})\big)\big(\boldsymbol{\nabla}_\alpha\tilde{V}_I(\mathbf{x},\mathbf{R}_I) - \boldsymbol{\nabla}_\alpha V_I(\mathbf{x},\mathbf{R}_I)\big) - \boldsymbol{\nabla}_\alpha\tilde{V}_I(\mathbf{x},\mathbf{R}_I)\tilde{b}_I(\mathbf{x},\mathbf{R}_I) \\ &+ \boldsymbol{\nabla}_\alpha V_I(\mathbf{x},\mathbf{R}_I)b_I(\mathbf{x},\mathbf{R}_I)\Big)\big(\mathbf{S}^{\mathrm{T}}\mathbf{x} - \mathbf{S}^{\mathrm{T}}\mathbf{R}_I\big)_\beta\,\mathrm{d}\mathbf{x} + \delta_{\alpha\beta}E_c(\mathbf{R})\,. \end{aligned} \tag{A.2}$$

As discussed in Appendix C, the contribution to the stress tensor arising from the self energy terms are not identically zero within the finite-difference approximation, and therefore have been retained to ensure the accuracy of the proposed formulation.

APPENDIX B

ON THE REFORMULATION OF THE STRESS TENSOR CONTRIBUTION $\sigma^{E_{NL}}$

In Section section 3.3, while deriving $\sigma^{E_{nl}}$—contribution to the stress tensor arising from the nonlocal pseudopotential energy—we have transferred the derivatives on the projectors (with respect to atomic position) to derivatives on the orbitals (with respect to space), as shown in Equation 3.9. This is because the orbitals are typically smoother than the projectors, and therefore the proposed strategy is expected to provide higher quality stresses, analogous to observations for the atomic forces [44, 45, 16]. To verify this, we consider an 8-atom unit cell of dc germanium and perform a Γ-point calculation. In Figure B.1, we plot the convergence of the stress tensor with and without the reformulation of $\sigma^{E_{nl}}$. It is clear from the results that the proposed formulation tremendously improves the accuracy of the stresses, and is therefore imperative to use in real-space DFT calculations.

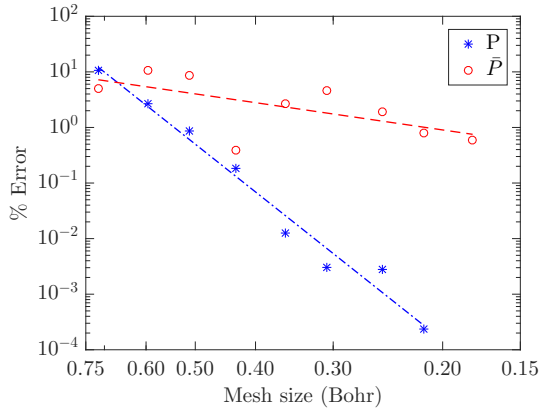

Figure B.1: Convergence of the stress tensor with mesh size for the dc germanium system with and without the nonlocal reformulation. The error is defined to be magnitude of the maximum difference in any component. The straight lines represent linear fits to the data.

APPENDIX C

ON THE STRESS TENSOR CONTRIBUTION $\sigma^{E_{SELF}}$ IN REAL-SPACE CALCULATIONS

As discussed in Section section 3.4, it can be shown analytically that $\sigma^{E_{self}} = 0$. However, due to the inexact nature of the chain rule within the finite-difference approximation, it is identically zero only in the limit of an infinitely fine mesh. In order to demonstrate the significant contribution of $\sigma^{E_{self}}$ in practical calculations, we consider an 8-atom unit cell of dc germanium and perform a Γ-point calculation. It is evident from the results presented in Figure C.1 that the proposed formulation of $\sigma^{E_{self}}$ tremendously improves the accuracy of the stresses, and is therefore imperative to use in real-space DFT calculations.

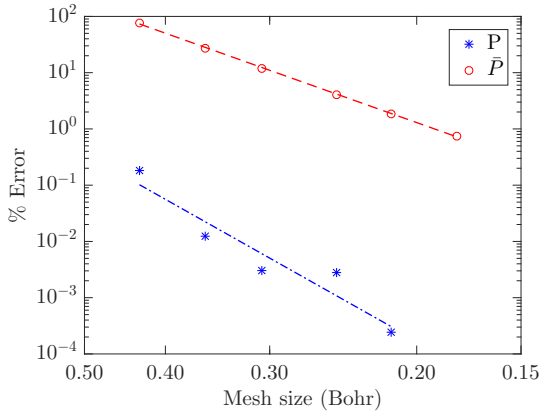

Figure C.1: Convergence of the stress tensor with mesh size for the dc germanium system with and without the contribution arising from the self energy. The error is defined to be magnitude of the maximum difference in any component. The straight lines represent linear fits to the data.

REFERENCES

[1] P. Hohenberg and W. Kohn, "Inhomogeneous electron gas," *Physical Review*, vol. 136, no. 3B, B864–B871, 1964.

[2] W. Kohn and L. J. Sham, "Self-consistent equations including exchange and correlation effects," *Physical Review*, vol. 140, no. 4A, A1133–A1138, 1965.

[3] G. Kresse and J. Furthmüller, "Efficient iterative schemes for ab initio total-energy calculations using a plane-wave basis set," *Physical Review B*, vol. 54, no. 16, pp. 11 169–11 186, 1996.

[4] M. D. Segall, P. J. D. Lindan, M. J. Probert, C. J. Pickard, P. J. Hasnip, S. J. Clark, and M. C. Payne, "First-principles simulation: Ideas, illustrations and the CASTEP code," *Journal of Physics: Condensed Matter*, vol. 14, no. 11, pp. 2717–2744, 2002.

[5] X. Gonze, B. Amadon, P. M. Anglade, J. M. Beuken, F. Bottin, P. Boulanger, F. Bruneval, D. Caliste, R. Caracas, M. Cote, *et al.*, "ABINIT: First-principles approach to material and nanosystem properties," *Computer Physics Communications*, vol. 180, no. 12, pp. 2582–2615, 2009.

[6] P. Giannozzi, S. Baroni, N. Bonini, M. Calandra, R. Car, C. Cavazzoni, D. Ceresoli, G. L. Chiarotti, M. Cococcioni, I. Dabo, A. Dal Corso, S. de Gironcoli, S. Fabris, G. Fratesi, R. Gebauer, U. Gerstmann, C. Gougoussis, A. Kokalj, M. Lazzeri, L. Martin-Samos, N. Marzari, F. Mauri, R. Mazzarello, S. Paolini, A. Pasquarello, L. Paulatto, C. Sbraccia, S. Scandolo, G. Sclauzero, A. P. Seitsonen, A. Smogunov, P. Umari, and R. M. Wentzcovitch, "QUANTUM ESPRESSO: A modular and open-source software project for quantum simulations of materials," *Journal of Physics: Condensed Matter*, vol. 21, no. 39, p. 395 502, 2009.

[7] S. Ismail-Beigi and T. A. Arias, "New algebraic formulation of density functional calculation," *Computer Physics Communications*, vol. 128, pp. 1–45, 2000.

[8] F. Gygi, "Architecture of qbox: A scalable first-principles molecular dynamics code," *IBM Journal of Research and Development*, vol. 52, no. 1.2, pp. 137–144, 2008.

[9] S. Goedecker, "Linear scaling electronic structure methods," *Rev. Mod. Phys.*, vol. 71, no. 4, pp. 1085–1123, Jul. 1999.

[10] D. R. Bowler and T. Miyazaki, "O(N) methods in electronic structure calculations," *Reports on Progress in Physics*, vol. 75, no. 3, p. 036 503, 2012.

[11] J. R. Chelikowsky, N. Troullier, and Y. Saad, "Finite-difference-pseudopotential method: Electronic structure calculations without a basis," *Physical Review Letters*, vol. 72, no. 8, pp. 1240–1243, 1994.

[12] A. Castro, H. Appel, M. Oliveira, C. A. Rozzi, X. Andrade, F. Lorenzen, M. A. L. Marques, E. K. U. Gross, and A. Rubio, "Octopus: A tool for the application of time-dependent density functional theory," *Physica Status Solidi B-Basic Solid State Physics*, vol. 243, no. 11, pp. 2465–2488, 2006.

[13] F. Shimojo, R. K. Kalia, A. Nakano, and P. Vashishta, "Linear-scaling density-functional-theory calculations of electronic structure based on real-space grids: Design, analysis, and scalability test of parallel algorithms," *Computer Physics Communications*, vol. 140, no. 3, pp. 303–314, 2001.

[14] J. I. Iwata, D. Takahashi, A. Oshiyama, T. Boku, K. Shiraishi, S. Okada, and K. Yabana, "A massively-parallel electronic-structure calculations based on real-space density functional theory," *Journal of Computational Physics*, vol. 229, pp. 2339–2363, 2010.

[15] S. Ghosh and P. Suryanarayana, "SPARC: Accurate and efficient finite-difference formulation and parallel implementation of density functional theory: Isolated clusters," *Computer Physics Communications*, vol. 212, pp. 189–204, 2017.

[16] S. Ghosh and P. Suryanarayana, "SPARC: Accurate and efficient finite-difference formulation and parallel implementation of density functional theory: Extended systems," *Computer Physics Communications*, vol. 216, pp. 109–125, 2017.

[17] Q. Xu, A. Sharma, B. Comer, H. Huang, E. Chow, A. J. Medford, J. E. Pask, and P. Suryanarayana, "SPARC: Simulation package for ab-initio real-space calculations," *arXiv preprint arXiv:2005.10431*, 2020.

[18] A. Sharma and P. Suryanarayana, "On real-space density functional theory for non-orthogonal crystal systems: Kronecker product formulation of the kinetic energy operator," *Chemical Physics Letters*, vol. 700, pp. 156–162, 2018.

[19] A. Natan, A. Benjamini, D. Naveh, L. Kronik, M. L. Tiago, S. P. Beckman, and J. R. Chelikowsky, "Real-space pseudopotential method for first principles calculations of general periodic and partially periodic systems," *Physical Review B*, vol. 78, no. 7, p. 075 109, 2008.

[20] R. Feynman, "Forces in molecules," *Physical Review Journals*, vol. 56, pp. 340–343, 1939.

[21] J. C. Slater, "Hellmann-Feynman and virial theorems in the x method," *The Journal of Chemical Physics*, vol. 57, p. 2389, 1972.

[22] J. F. Janak, "Simplification of total-energy and pressure calculations in solids," *Physical Review B*, vol. 9, p. 3985, 1974.

[23] M. T. Yin, "Pressure and virial theorem in pseudopotential formalism," *Physical Review B*, vol. 27, p. 7769, 1983.

[24] O. H. Nielsen and R. M. Martin, "Quantum-mechanical theory of stress and force," *Physical Review B*, vol. 32, p. 3780, 1985.

[25] O. H. Nielsen and R. M. Martin, "Stresses in semiconductors: Ab initio calculations on si, ge, and gaas," *Physical Review B*, vol. 32, p. 3792, 1985.

[26] A. D. Corso and R. Resta, "Density-functional theory of macroscopic stress: Gradient-corrected calculations for crystalline se," *Physical Review B*, vol. 50, p. 4327, 1994.

[27] T. Thonhauser, C. Ambrosch-Draxl, and D. J. Singh, "Stress and pressure within the linearized-augmented plane-wave method," *Solid State Communications*, vol. 124, pp. 275–282, 2002.

[28] M. Torrent, F. Jollet, F. Bottin, G. Zérah, and X. Gonze, "Implementation of the projector augmented-wave method in the ABINIT code: Application to the study of iron under pressure," *Computational Materials Science*, vol. 42, pp. 337–351, 2008.

[29] K. N. Kudin and G. E. Scuseria, "Analytic stress tensor with the periodic fast multipole method," *Physical Review B*, vol. 61, p. 5141, 2000.

[30] J. Soler, E. Artacho, J. D. Gale, A. García, J. Junquera, P. Ordejón, and D. Sánchez-Portal, "The SIESTA method for ab initio order-n materials simulation," *Journal of Physics: Condensed Matter*, vol. 14, no. 11, 2002.

[31] F. Knuth, C. Carbogno, V. Atalla, V. Blum, and M. Scheffler, "All-electron formalism for total energy strain derivatives and stress tensor components for numeric atom-centered orbitals," *Computer Physics Communications*, vol. 190, pp. 33–50, 2015.

[32] P. Motamarri and V. Gavini, "Configurational forces in electronic structure calculations using kohn-sham density functional theory," *Physical Review B*, vol. 97, p. 165 132, 2018.

[33] A. Sharma and P. Suryanarayana, "On the calculation of the stress tensor in real-space Kohn-Sham density functional theory," *The Journal of chemical physics*, vol. 149, no. 19, p. 194 104, 2018.

[34] P. Suryanarayana, P. P. Pratapa, A. Sharma, and J. E. Pask, "SQDFT: Spectral quadrature method for large-scale parallel O(N) Kohn–Sham calculations at high temperature," *Computer Physics Communications*, vol. 224, pp. 288–298, 2017.

[35] A. Sharma, S. Hamel, M. Bethkenhagen, J. E. Pask, and P. Suryanarayana, "Real-space formulation of the stress tensor for O(N) density functional theory: Application to high temperature calculations," *The Journal of Chemical Physics*, vol. 153, no. 3, p. 034 112, 2020.

[36] N. D. Mermin, "Thermal properties of the inhomogeneous electron gas," *Phys. Rev.*, vol. 137, no. 5A, A1441, 1965.

[37] J. E. Pask and P. A. Sterne, "Real-space formulation of the electrostatic potential and total energy of solids," *Phys. Rev. B*, vol. 71, p. 113 101, 11 Mar. 2005.

[38] P. Suryanarayana, V. Gavini, T. Blesgen, K. Bhattacharya, and M. Ortiz, "Non-periodic finite-element formulation of Kohn-Sham density functional theory," *J Mech Phys Solids*, vol. 58, no. 2, pp. 256–280, 2010.

[39] D. C. Langreth and J. P. Perdew, "Theory of nonuniform electronic systems. i. analysis of the gradient approximation and a generalization that works," *Phys. Rev. B*, vol. 21, no. 12, p. 5469, 1980.

[40] D. C. Langreth and M. Mehl, "Easily implementable nonlocal exchange-correlation energy functional," *Phys. Rev. Lett.*, vol. 47, no. 6, p. 446, 1981.

[41] L. Kleinman and D. Bylander, "Efficacious form for model pseudopotentials," *Phys. Rev. Lett.*, vol. 48, no. 20, p. 1425, 1982.

[42] P. Suryanarayana and D. Phanish, "Augmented Lagrangian formulation of orbital-free density functional theory," *J. Comput. Phys.*, vol. 275, no. 0, pp. 524–538, 2014.

[43] S. Ghosh and P. Suryanarayana, "Higher-order finite-difference formulation of periodic orbital-free density functional theory," *J. Comput. Phys.*, vol. 307, pp. 634–652, 2016.

[44] K. Hirose, T. Ono, Y. Fujimoto, and S. Tsukamoto, *First-principles calculations in real-space formalism*, 2005.

[45] X. Andrade, D. Strubbe, U. De Giovannini, A. H. Larsen, M. J. Oliveira, J. Alberdi-Rodriguez, A. Varas, I. Theophilou, N. Helbig, M. J. Verstraete, *et al.*, "Real-space grids and the octopus code as tools for the development of new simulation approaches for electronic systems," *Physical Chemistry Chemical Physics*, vol. 17, no. 47, pp. 31 371–31 396, 2015.

[46] P. Focher, *First-principle studies of structural phase transformations*. ISAS, 1994.

[47] Q. Xu, A. Sharma, and P. Suryanarayana, "M-SPARC: Matlab-simulation package for ab-initio real-space calculations," *SoftwareX*, vol. 11, p. 100 423, 2020.

[48] P. P. Pratapa, P. Suryanarayana, and J. E. Pask, "Anderson acceleration of the Jacobi iterative method: An efficient alternative to Krylov methods for large, sparse linear systems," *J. Comput. Phys.*, vol. 306, pp. 43–54, 2016.

[49] P. Suryanarayana, P. P. Pratapa, and J. E. Pask, "Alternating Anderson-Richardson method: An efficient alternative to preconditioned Krylov methods for large, sparse linear systems," *arXiv preprint arXiv:1606.08740*, 2016.

[50] Y. Zhou, Y. Saad, M. L. Tiago, and J. R. Chelikowsky, "Parallel self-consistent-field calculations via Chebyshev-filtered subspace acceleration," *Physical Review E*, vol. 74, no. 6, p. 066 704, 2006.

[51] Y. Zhou, Y. Saad, M. L. Tiago, and J. R. Chelikowsky, "Self-consistent-field calculations using Chebyshev-filtered subspace iteration," *Journal of Computational Physics*, vol. 219, no. 1, pp. 172–184, 2006.

[52] P. P. Pratapa and P. Suryanarayana, "Restarted Pulay mixing for efficient and robust acceleration of fixed-point iterations," *Chemical Physics Letters*, vol. 635, pp. 69–74, 2015.

[53] A. S. Banerjee, P. Suryanarayana, and J. E. Pask, "Periodic Pulay method for robust and efficient convergence acceleration of self-consistent field iterations," *Chem. Phys. Lett.*, vol. 647, pp. 31–35, 2016.

[54] N. Troullier and J. L. Martins, "Efficient pseudopotentials for plane-wave calculations," *Physical Review B*, vol. 43, no. 3, pp. 1993–2006, 1991.

[55] H. J. Monkhorst and J. D. Pack, "Special points for Brillouin-zone integrations," *Phys. Rev. B*, vol. 13, p. 5188, 12 1976.

[56] J. P. Perdew and Y. Wang, "Accurate and simple analytic representation of the electron-gas correlation energy," *Physical Review B*, vol. 45, no. 23, pp. 13 244–13 249, 1992.

[57] J. P. Perdew, K. Burke, and M. Ernzerhof, "Generalized gradient approximation made simple," *Phys. Rev. Lett.*, vol. 77, no. 18, p. 3865, 1996.

[58] X. Gonze, J. .-M. Beuken, R. Caracas, F. Detraux, M. Fuchs, G. .-M. Rignanese, L. Sindic, M. Verstraete, G. Zerah, F. Jollet, M. Torrent, A. Roy, M. Mikami, P. Ghosez, J. .-Y. Raty, and D. C. Allan, "First-principles computation of material properties: The ABINIT software project," *Comp. Mater. Sci.*, vol. 25, 478–492(15), 2002.

[59] P. Pulay, "Ab initio calculation of force constants and equilibrium geometries in polyatomic molecules," *Molecular Physics*, vol. 17, pp. 197–204, 1969.